Simulation Environment for an Open-Ended Coaxial Probe and Visualisation of Permittivity Measurements

Bachelor Thesis

Bart Hettema
Wietse Bouwmeester

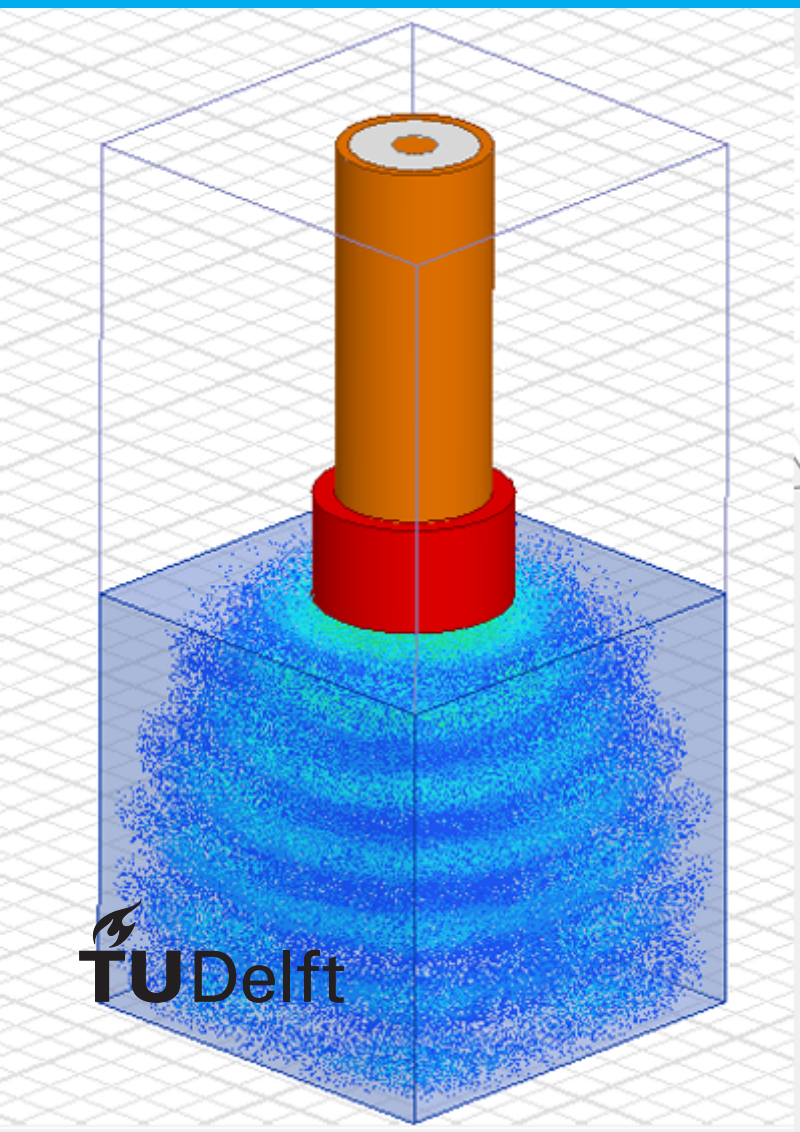

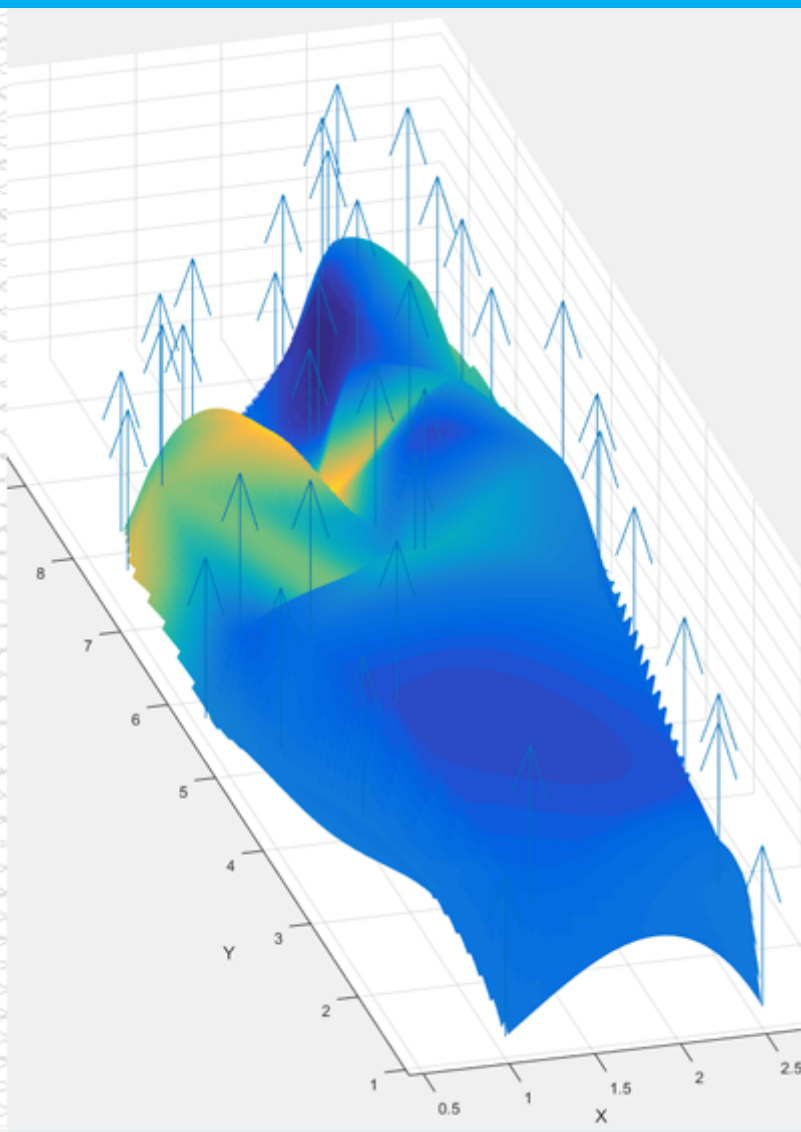

Simulation Environment for an Open-Ended Coaxial Probe and Visualisation of Permittivity Measurements

Bachelor Thesis

by

Bart Hettema
Wietse Bouwmeester

24 June 2016

Students:	Bart Hettema	4293398
	Wietse Bouwmeester	4300807
Project duration:	April 18, 2016 – July 1, 2016	
Supervisor:	dr. Marco Spirito,	TU Delft

TU Delft

Abstract

This thesis work focuses on the development of reference data and visualization software to implement a user friendly probe to image the electrical parameters (i.e., permittivity) of biological materials, such as the skin.

The reference data is used for the creation of a lookup table that can be used to quickly derive the relative permittivity of a material from the probe measurements. It was found that the reference data provided for the lookup table resulted in reliable derivation of relative permittivity.

A second task described in this report is the design and implementation of a graphical user interface which displays measured relative permittivity values. This user interface should be capable of interacting with the measuring equipment and positioning system to acquire data and corresponding positions. The user interface is capable of presenting these in a visual format by showing 2D and 3D plots of the values and the locations at which they were measured. The underlying design pattern is explained. The user interface, written in MATLAB, is fully Object Oriented and uses the Model-View-Controller paradigm. The permittivity values can be viewed at different frequencies and a choice to view the magnitude, the real part or the imaginary part of the permittivity can be made. A modular approach has made the user interface well extendible.

Contents

1 Introduction

1.1. Background

In the Netherlands alone, in 2015 almost fifteen thousand people were diagnosed with skin cancer [1]. Skin cancer occurs in different typologies, among the most common are melanoma and squamous cell carcinoma. Medical research has repeatedly shown [2] that the early detection of cancer is crucial to obtain high survival rates. The Breslow depth (table 1.1) [3], which is the thickness of tumour cells, is often used as the quantifying parameter to determine the chance of survival.

Table 1.1: Breslow depth and survival rates

Thickness	5-year survival
< 1 mm	95 % to 100 %
1 mm to 2 mm	80 % to 96 %
2,1 mm to 4 mm	60 % to 75 %
> 4 mm	37 % to 50 %

The identification of a malignant cancer is a complex and expensive process since it is subject to the availability of experienced, trained dermatologists, usage of surgical rooms for partial excision of the skin an laboratories to analyse the tissue. In the case of squamous cell carcinoma, this form is easier to spot, but harder to remove. This cancer is surgically removed layer by layer. Every layer needs to be checked for traces of remaining carcinoma by freezing it and examining it using microscopes. This is a very tedious process that could greatly benefit from an instrument that can quickly detect if there are carcinoma traces remaining in the skin, even without excising it.

An instrument that can detect traces of malignant melanoma has the potential to revolutionize the way skin cancer is treated. For example general practitioners could use such an instrument to check if a melanoma is malignant and excise it without the need to send the patient to an experienced dermatologist. The surgeon removing squamous cell carcinoma also benefits greatly by detecting which pieces of skin are cancer free and which are not so that he or she has to excise less.

1.2. Overview of the project

1.2.1. Subsystems

This project revolves around a probe system which, ultimately, should be able to detect skin cancer. This system has been named the Tissue Imaging Probe System (TIPS). There are three main parts within this project: readout and calibration of the probe, tracking the position of the probe, and visualising the data. This report describes part of the readout and calibration and describes the visualisation.

Truong and Kremers [4] describe the readout and calibration more in detail, and Treffers and Wietmarschen [5] have researched the tracking of the position of the probe.

The probe is an open-ended coaxial probe, which is essentially a cut-off coaxial cable. The dielectric material on the inside is soft Teflon. To protect the dielectric a cap is added on the probe. The probe has a flat, round surface. This skin, however, is seldom really flat. Because an air gap could negatively impact the measurement, an interface gel between the skin and the probe will be used to fill in the air gaps. The effects of the cap, gel and air gap are simulated and described in this report.

1.2.2. Permittivity

The measuring system aims to detect differences in the skin. The skin property that is compared is its relative permittivity. The permittivity (ε) indicates the resistance of a material to the forming of an electric field. The permittivity can be a complex value. ε' denotes the real part of the permittivity, while ε'' is the symbol for the imaginary part, see eq. (1.1). The relative permittivity (ε_r) of a material is the ratio of the permittivity of the material to the permittivity of vacuum (ε_0). The relative permittivity is also known as the dielectric constant, although this term is deprecated [6, p. 6].

$$\varepsilon = \varepsilon_0 \varepsilon_r = \varepsilon' + \mathrm{j}\varepsilon'' \tag{1.1}$$

1.2.3. Scattering parameters

The simulation will use scattering parameters to calculate the relative permittivities. Scattering parameters (S-parameters) are a set of parameters that relate to the reflection of a wave in a transmission line [7]. The size of the S-matrix depends on the number of ports a system has. An one port has an 1 by 1 S-matrix, while a two port has a 2 by 2 S-matrix and a three a 3 by 3 matrix. The S-parameters relate the scattered waves of a two-port network, as shown in fig. 1.1, to the incident waves:

$$\begin{bmatrix} b_1 \\ b_2 \end{bmatrix} \begin{bmatrix} S_{11} & S_{12} \\ S_{21} & S_{22} \end{bmatrix} = \begin{bmatrix} a_1 \\ a_2 \end{bmatrix} \tag{1.2}$$

where a_1 and a_2 are the incident waves, b_1 and b_2 the scattered waves, respectively, and S_{11}, S_{12}, S_{21} and S_{22} the S-parameters. Another name for the S_{11} parameter, is reflection coefficient.

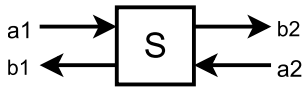

Figure 1.1: Two port network with incoming and outgoing waves

The S-parameters and impedance parameters are part of the same family of electrical parameters. They are closely related to each other by eq. (1.3). In this equation 1_N is a N by N identity matrix and $\sqrt{z}$ is a N by N diagonal matrix with the characteristic impedance of the ports on the diagonal.

$$Z = \sqrt{z}(1_N + S)(1_N - S)^{-1}\sqrt{z} \tag{1.3}$$

S-parameters are therefore just another way to represent impedance.

1.3. Problem definition

The main research question of this project is how to cost effectively identify skin cancer. The detection of the skin cancer using electromagnetic waves is based upon the fact that the relative permittivity of cancerous skin is different from that of healthy skin. The permittivity of the skin is mainly dependant on the water content of the skin, since water has a high permittivity and makes up about 64% of the skin [8]. Tumour cells have a higher water content [9] and can thus be detected by their higher permittivity. This is the material property that the measurement instrument will be using to detect non-healthy skin. The main research question, within the scope of this thesis, is divided in the following sub-questions:

- How to derive the relative permittivity from the measured wave properties?

- What is the effect of interface gel on the measurements?
- What is the effect of an protective cap on the probe used for the measurements?
- How to best present the data to the user of the instrument?

1.4. Programme of requirements

1.4.1. Simulations

- A simulation environment, using commercial tools, that solves electromagnetic problems in a defined environment should be implemented.
- The environment should include all the key effects to properly reproduce the values that will be used to perform the calibration of the instrument, which is the impedance.
- The environment should be able to run in a reasonable time: a day, and preferably less.
- The simulations should be able to show the effects of an interface gel between the skin and the probe.
- The simulations should show the effect of an interface cap between the probe and the skin.
- The output of the simulations can be used to calibrate the measurement equipment.
- The interface gel and probe cap should not be dangerous to humans and human skin.

1.4.2. Graphical User Interface

- The user should be able to interact with the data visualisation.
- The data visualisation should be intuitive and easy to use.
- The data visualisation should be able to display the measured relative permittivity in a manner which clearly shows the measured value at a location.
- The data visualisation should be able to display all the measured data, which includes the magnitude, real part and imaginary part of the complex permittivity at different frequencies.
- The data visualisation should be able to show measurement data of a specific measurement point by clicking on it
- The data visualisation should update the plotted data in real time, so the user always knows the current state of the measurement.

1.5. Report structure

This report first explains the simulation used in section 2.1. From this follows the derivation of the simulation data used for the calibration of the measurement instrument in section 2.2. Section 2.3 describes how to construct the reference data for the measuring system. Sections 2.4 and 2.5 are the last sections on simulation and show the effect of a cap on the probe and the use of an interface gel.

Then the data visualisation is discussed. Section 3.1 describes the design pattern and the code structure of the user interface The next section, section 3.2, shows what features are implemented in the user interface. Lastly, section 3.3 discusses various ways to present the data, after which the conclusion follows in chapter 4.

2

Skin interface

2.1. Simulation

In order to accurately convert impedance, which is measured by the instrument, into permittivity data which is used for tumour identification, an accurate model of the probe is required.

To realize such a model, the approach chosen in this thesis work is to make use of accurate three dimensional (3D) electromagnetic simulation software. By replicating the probe in the simulation environment, see fig. 2.2, a link between impedance and permittivity can be established. This link can then be used to achieve accurate calibration in the real world and impedance can be related back to permittivity, which in turn can be used to identify anomalies in the skin tissue.

The simulation of the system is done using Ansoft High Frequency Structure Simulation, HFSS for short. The version that is used is version is 13.0. This software was chosen since it is a stable commercial platform which was available within the group this research activity was carried out in.

HFSS calculates S-parameters of the models it is given. The way HFSS calculates the S-parameters of the design it is given, is by dividing the design in tetrahedrons in a process called meshing and then numerically solving the Maxwell equations using this mesh. In order to obtain accurate solutions, HFSS refines the mesh of the model iteratively until a user-defined error margin is reached. This process is called adaptive meshing. When a mesh is found that meets the requirements, it then starts a frequency sweep to obtain solutions for a specified frequency range.

2.1.1. Setting up the simulation

To set up the simulation, first the coaxial cable was created by drawing three cylinders and subtracting them from each other. The dimensions of the coaxial cable are displayed in fig. 2.1. These dimensions were obtained by measuring the coaxial probe that was going to be used for the measurements. After that, the air box and the skin material were drawn.

Now boundary conditions and excitations needed to be assigned. An excitation is a surface area that acts as the source of energy for the simulated system. At the excitation boundary the electric field is fixed by the user settings. The excitation boundary is also the surface HFSS will calculate the S-parameters at. The surface the excitation was defined at was the dielectric on top of the probe. Since a coaxial probe is used, the excitation was defined to be a wave port excitation and set to a TEM mode, this means that the electric and magnetic waves are perpendicular to the direction of propagation.

Next, the faces of the air box and the skin material on the outside of the model were assigned the radiation boundary condition. This condition emulates infinite space around the design and thus ensuring no reflections from the outer faces of the model occur.

If this boundary condition is not assigned, HFSS will assume the perfect E boundary condition. This condition can be imagined as a shell of a perfect conducting material covering the outside faces of

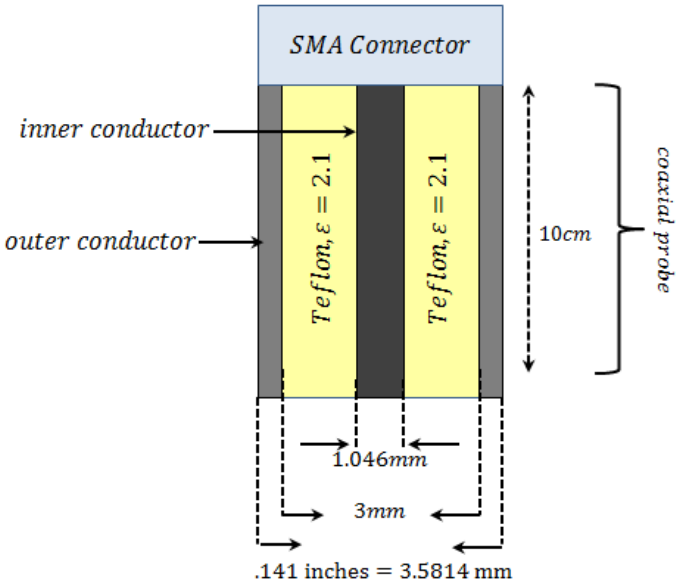

Figure 2.1: Dimensions of the coaxial cable

the design. This is in this case not desired since it does not reflect the real situation, contrary to the radiation boundary condition which does this much better. A picture of the completed simulation model is shown in fig. 2.2.

Lastly, the analysis was set up so that a sweep from 0,5 GHz to 20 GHz in steps of 0,1 GHz was performed.

The simulation that has been described above provides the S-parameters as measured at the top of the coaxial probe. However, the S-parameters at the bottom of the coaxial probe are desired. So the measurement plane needs to be "shifted" down. This process is called de-embedding, a graphical rendering of the process is displayed in fig. 2.3. This is done by calculating the S-matrix of the coaxial probe and this S-matrix can then be used to remove the effects of the probe from the measurements. The de-embedding process is described more in detail by Truong and Kremers [4].

The S-matrix can be calculated by removing everything from the simulation but the coaxial cable. Another wave port excitation can be defined at the bottom of the coaxial probe and HFSS will now calculate the complete two port S-matrix instead only the reflection coefficients.

The other simulations made within this project are all adapted from the general setup described in this section.

2.1.2. Optimization

The HFSS simulations can take a very long time when a system is not optimized for this task. Since the simulations were run on a laptop, the model needs to be optimized in order to make simulations run in a reasonable time. For reference, the specifications of the laptop are as follows: an i7-4700MQ CPU running nominally at 2,40 GHz with 8 GB of Random Access Memory. Also, the laptop is running Windows 10.

It was observed that simulation time dramatically increases with choosing a higher solution frequency. Because the wave varies more spatially when frequency becomes higher (wavelength becomes shorter), smaller tetrahedrons need to be used in the mesh to get accurate solutions. This has as a result that the mesh becomes finer and therefore increases the simulation time. Also it was found that simulation time increases by increasing the relative permittivity of the skin material. This can be seen by looking at eq. (2.1).

$$\lambda = \frac{c_0}{f\sqrt{\epsilon_r}} \tag{2.1}$$

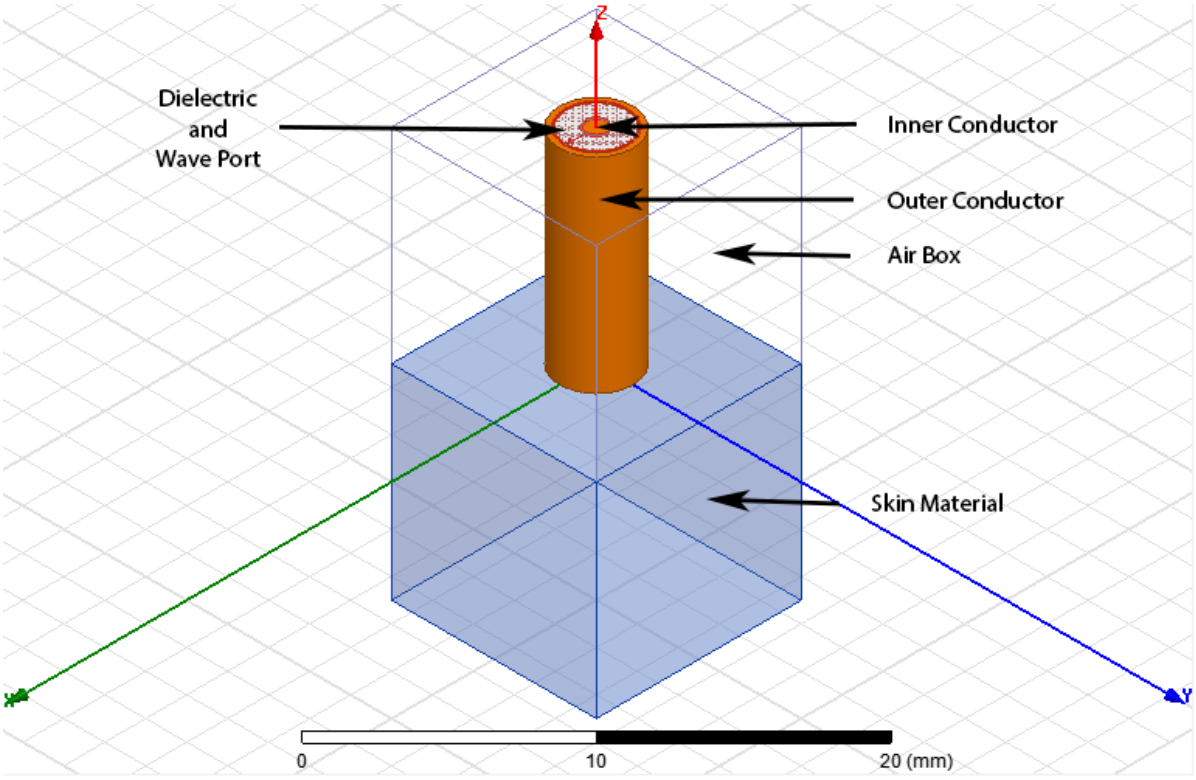

Figure 2.2: The model of the general setup described in section 2.1.1

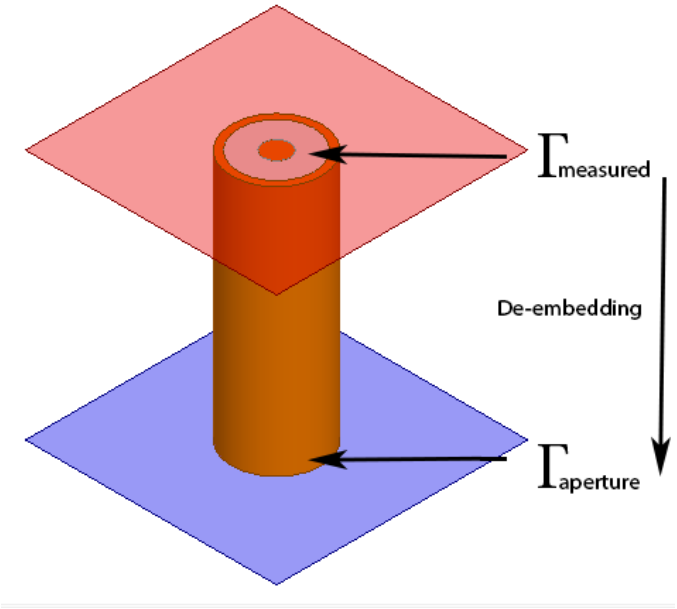

Figure 2.3: The de-embedding process

When the relative permittivity increases, the wavelength decreases. This again causes the need for a finer mesh and thus increasing simulation time as well.

An effective way to optimize the simulation, is by reducing the mesh size. Choosing smaller model dimensions and thereby reducing volume is a great way to reduce the mesh size. This comes at the cost of an error in the calculated S-parameters since the model now reflects the situation in reality less well. To determine the effect of reducing the simulation volume, various simulation designs were created with varying width and length of the skin material and air box. These designs were solved with skin permittivity of 20, a solution frequency of 3,5 GHz and a sweep from 0,5 GHz to 3,5 GHz.

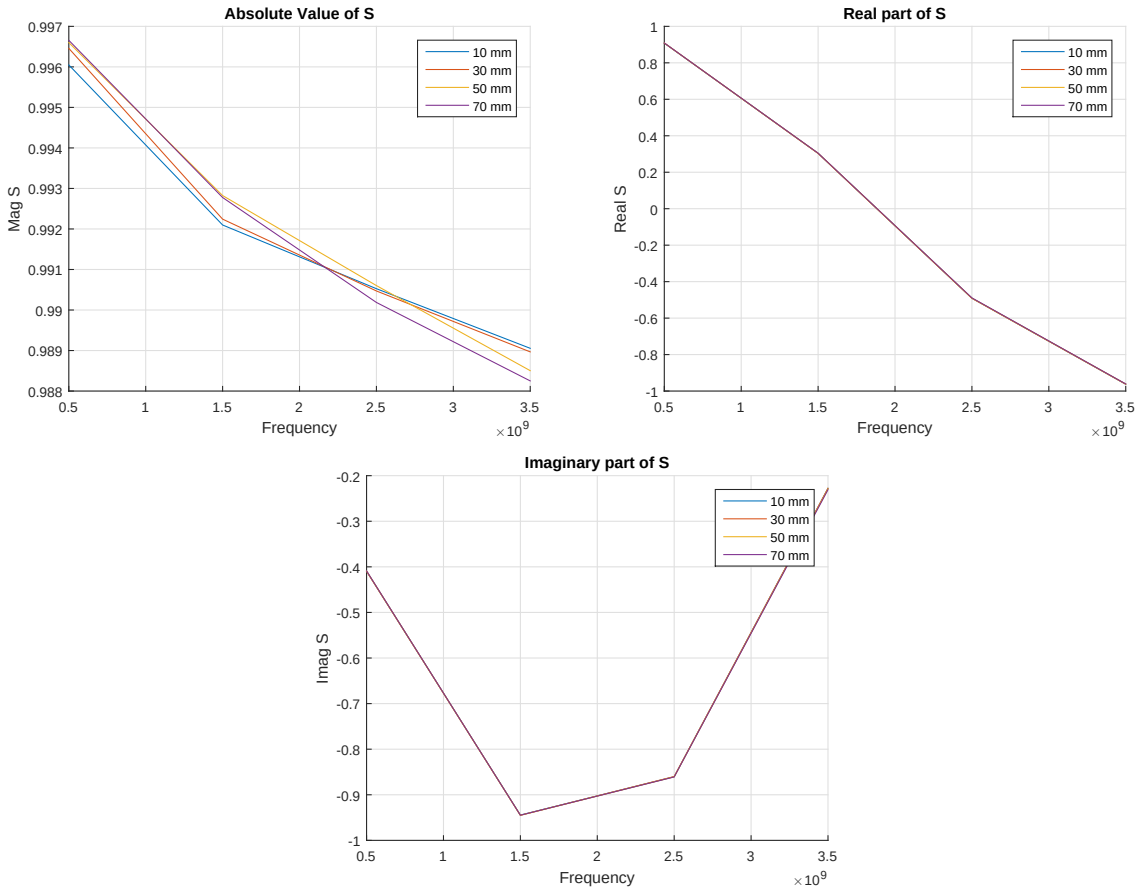

Figure 2.4: The calculated S-parameters using a cube of skin with width and length varying between 10 mm × 10 mm and 70 mm × 70 mm

Figure 2.4 shows that scaling down the design from 70 mm by 70 mm to 10 mm by 10 mm almost makes no difference at all. The biggest difference that was found between 10 mm × 10 mm and 70 mm × 70 mm is 0.003 (the imaginary component at 3,5 GHz), which is well below the set convergence. Therefore the design can be shrunk down, and simulation times can be reduced to acceptable durations.

2.2. Derivation of standard coefficients

To do measurements, a Vector Network Analyser, VNA for short, was used. This instrument measures the impedance versus frequency.

The calibration procedure of one port for this instrument normally uses three devices called standards. These standards can be attached to the probe. The frequency responses of these standards are known and by measuring these with the VNA, the statistical error of the VNA can be computed. By solving a set of linear equations, the so called standard coefficients can be found. These coefficients can then be used to remove the statistical error from the measurements. This correction process is described more in detail by Truong and Kremers [4].

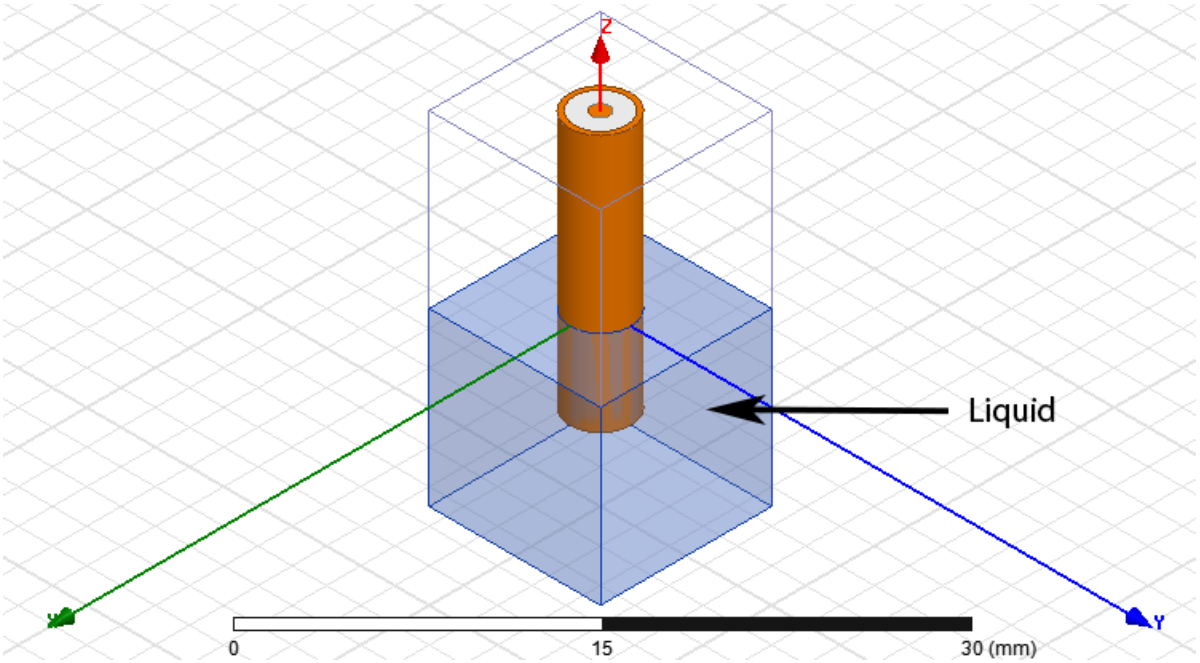

Figure 2.5: The design for generating the S-parameters for calculating the error terms

Since the probe used for the measurements is non-connectorized, which means it is not possible to connect loads to the probe, the choice was made to use three different liquids as standards.

HFSS was used to generate the frequency response for these standard liquids for the specific geometry of the non-connectorized probe. This was done by setting the relative permittivities of the liquids to reference permittivities that were provided to our team. The reference permittivities were obtained by measurements performed with a calibrated VNA. The generated dataset was de-embedded and used as the input for the standard coefficient calculation algorithm by Truong and Kremers [4].

2.2.1. Setting up the simulation

The general model described in section 2.1.1 was adapted by extending the coaxial cable into the skin material, which now represented the liquid. A picture of the simulation geometry can be seen in fig. 2.5.

The de-embedding model was adjusted as well by increasing the length of the probe so that it matches that of the probe submerged in liquid.

Now the permittivity of the liquids needed to be assigned. HFSS does not have ε'' material parameter. Instead of this HFSS has a dielectric loss tangent material parameter, so a conversion needed to be done.

2.2.2. Conversion from ε' to dielectric loss tangent

The dielectric loss tangent can be calculated from ε' and ε''. Since the file contained quite some measurement points, this process was automated using MATLAB rather than doing it by hand. First the measured permittivity data was copied into a MATLAB matrix. The first column contained the frequency, the second ε' and the third ε''. Using the relationship described in eq. (2.2), the dielectric loss tangent can be calculated.

$$\tan\sigma = \frac{\varepsilon''}{\varepsilon'} \tag{2.2}$$

For every measured frequency point, the frequency along with the ε' was written to a file and the frequency along with the ε'' was written to another separate file. In both files, the frequency and the permittivity data were spaced using tabs. Files of this format can be easily imported into HFSS as

datasets. These datasets could then be assigned to the relative permittivity and the dielectric loss tangent material parameters of the three liquids. Now the simulations were ready to be executed and with the generated S-parameters and the S-parameters from the de-embedding the error terms could be calculated.

The code for converting to the dielectric loss tangent can be found in appendix A.1.1. `[FILENAME]` should be replaced with appropriate file names.

2.2.3. Results

In figures 2.6 to 2.8 the calculated S-parameters alongside the relative permittivity of the three liquids are shown.

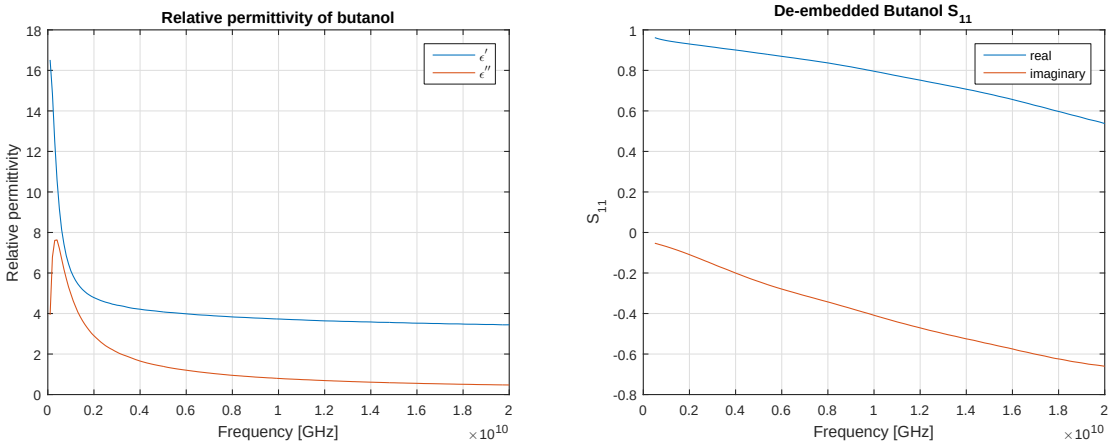

Figure 2.6: The permittivity and S-parameters of butanol

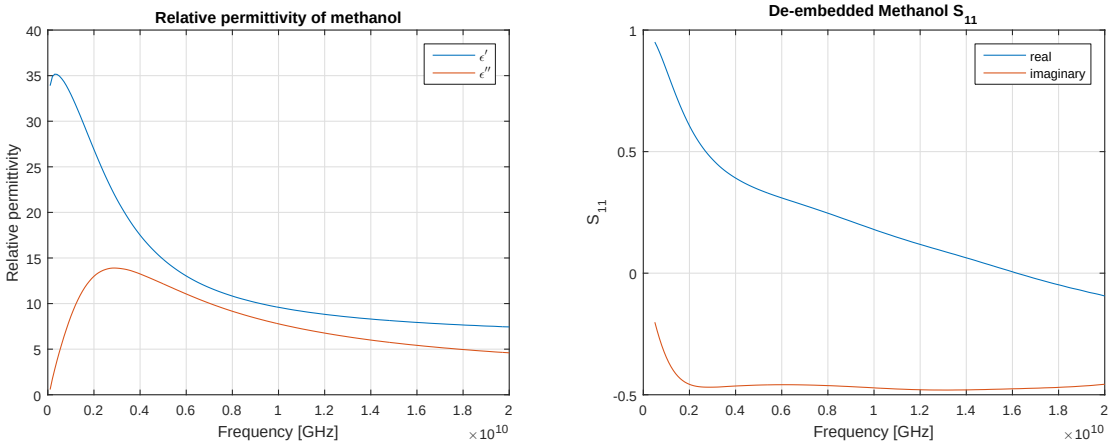

Figure 2.7: The permittivity and S-parameters of methanol

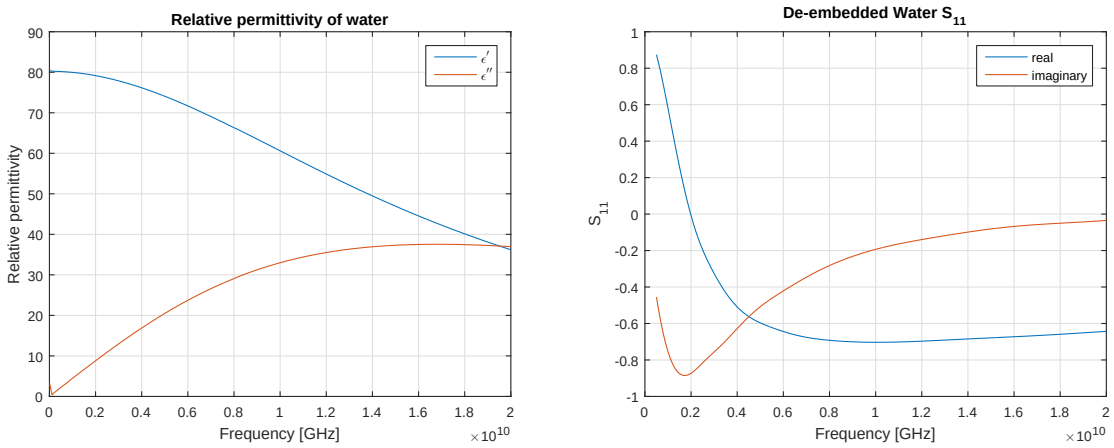

Figure 2.8: The permittivity and S-parameters of water

2.3. Lookup table reference data

The measurements done with the probe only result in S-parameters. To determine the relative permittivity from these S-parameters, the S-parameters need to be processed. This can be done by using a mathematical model [10] or by using a lookup table. Because creating the mathematical model is quite complicated and beyond the scope of this bachelor project, the lookup table method was chosen.

The lookup table consists out of a matrix of S-parameters for various relative permittivities varying with frequency generated using HFSS. A MATLAB script takes the measured S-parameters and uses linear interpolation to derive the relative permittivity of the measured material. More in-depth info can be found in Truong and Kremers [4]. A picture of the lookup table is displayed in fig. 2.9.

2.3.1. Setting up the simulation

The general setup from section 2.1.1 was modified by setting up a sweep that would vary the real part of the relative skin permittivity from 1 to 40.

The upper limit of 40 was chosen because in a range from 0,5 GHz to 20 GHz the maximum of the relative permittivity of skin is about 45 at 0,5 GHz [11]. A value of 40 was deemed to be high enough since simulation time constraints (simulation time increases with increasing relative permittivity) and the fact that the relative skin permittivity quickly drops below 40 after about 1 GHz [11]. The lower limit at a relative permittivity of 1 was used since low values of permittivity do not take that much time to simulate and to be able to plot permittivities of butanol and methanol that were used to calculate the error terms.

2.3.2. Complex relative permittivity

The above described approach only generates data for looking up the real part of the relative permittivity. The drawback of this approach is that the imaginary part of the relative permittivity can not be derived. To enable looking up the imaginary part too, new data for the lookup table needed to be generated. The lookup table script needed to be upgraded to support the new dataset with imaginary parts of the relative permittivity as well. Truong and Kremers [4] show how this is done.

To generate this dataset, a sweep over the imaginary part of the relative permittivities was set up for every value of the real part of the relative permittivity. The range of the sweep over the imaginary part of the relative permittivities was chosen to be from 0 to 15. This is because to be able to accommodate methanol and butanol in the plot. Methanol and butanol both are within this range [12].

In order to reduce computing time, the choice was made to reduce the number of simulation points. Instead of sweeping the real part of the relative permittivity in steps of 1 and the frequency in steps of 0,1 GHz, it was chosen to sweep the permittivity in steps of 2 and the frequency in steps of 1 GHz

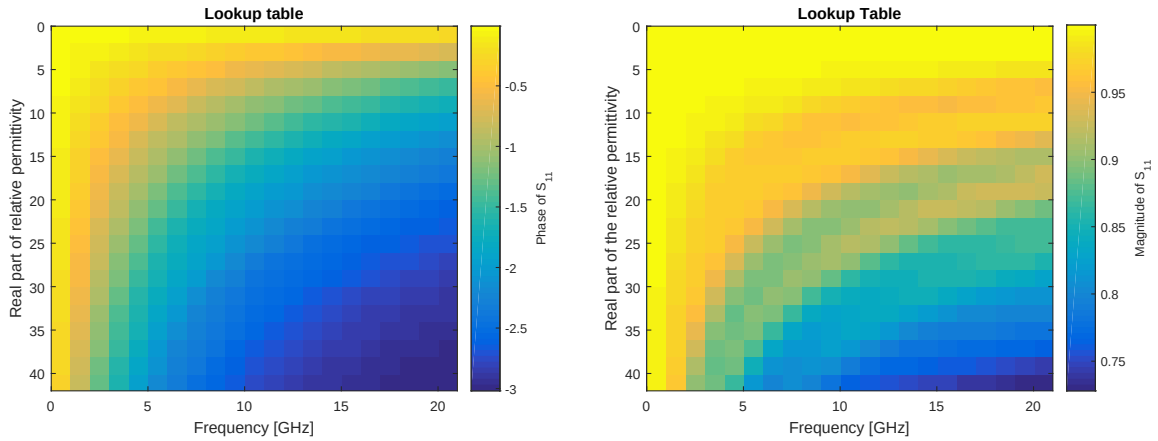

Figure 2.9: Lookup table for S-parameters. The colours indicate the phase (left) and the magnitude (right) of the S-parameters. The MATLAB script will match the measured S-parameter to the correct phase and magnitude of the S-parameters in the lookup table at every frequency and in this way the real part of the relative permittivity is plotted

from 0,5 GHz to 20,5 GHz. With these settings, generating the complex lookup table data should take approximately equally long as the real lookup table data.

2.3.3. Setting up the simulation for complex relative permittivities

HFSS only accepts the dielectric loss tangent and not the imaginary part of the relative permittivity. HFSS is only able to sweep the variables it knows of in regular steps and since the dielectric loss tangent is not linearly related to the imaginary part of the complex relative permittivity, a normal sweep can not be used.

Instead, the option to add a parametric sweep from a file was used. The MATLAB script used to convert to the dielectric loss tangent from the complex relative permittivity was modified (appendix A.1.2) to generate the desired sweep settings that could then be imported into HFSS.

2.3.4. Results

In the figures 2.10 and 2.11 are some plots of the data generated for the lookup table displayed. Only five of the real permittivity variations and five of the imaginary permittivity variations are shown to increase readability.

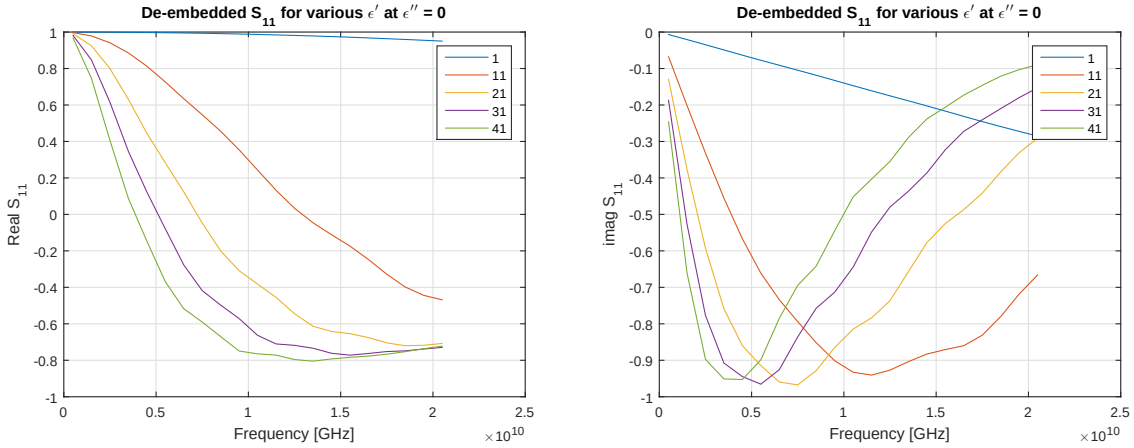

Figure 2.10: Plots of the de-embedded S-parameters for several of the many ε' while ε'' was kept constant at 0

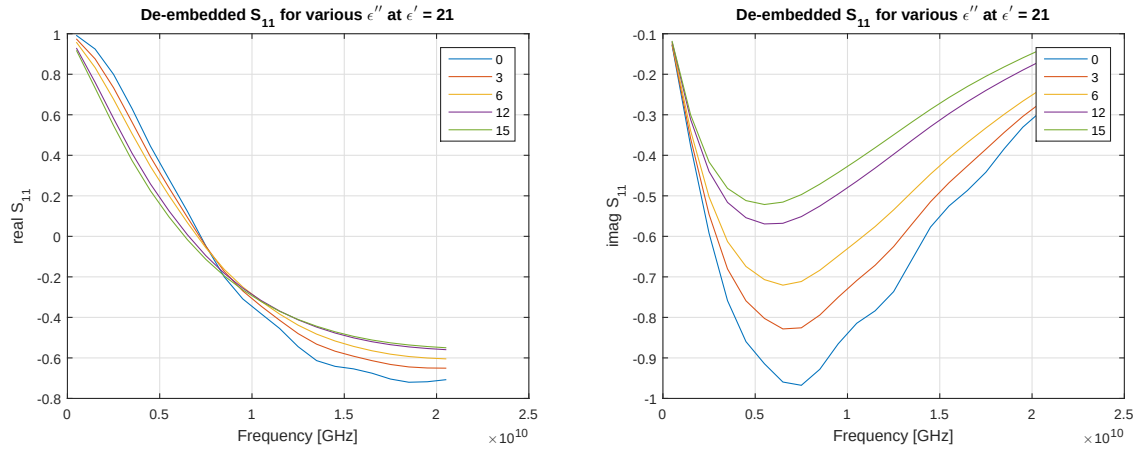

Figure 2.11: Plots of the de-embedded S-parameters for several of the many ε'' while ε' was kept constant at 21

2.4. Effect of interface gel

When measuring the skin, it is almost unavoidable to have some air pockets between the probe and the skin due to hairs and other inconsistencies of the skin. This problem can be modelled by two capacitances connected in series. The first capacitance is the one caused by the air pockets and the second one is the capacitance of the skin. The capacitance of interest is the capacitance of the skin.

The impedance of a capacitor at a specific frequency is given by eq. (2.3). This equation shows that the impedance, Z, increases with decreasing capacitance, C. ω is the angular velocity.

$$Z = \frac{1}{j\omega C} \tag{2.3}$$

If the capacitances are approximated as parallel plate capacitors, it can be seen in eq. (2.4) that with decreasing relative permittivity ε_r, the capacitance decreases. In this formula d and A are respectively the distance between the contacts and the surface area of the contacts.

$$C = \frac{\varepsilon_r \varepsilon_0 A}{d} \tag{2.4}$$

It thus is observed that if there is air present, which has a relative permittivity of 1, there is a small capacitance between the skin and the probe which in turn is a large impedance.

Since this impedance is large, the impedance causes a large voltage drop relative to the skin impedance. Therefore, it is harder to measure the quantity of interest.

To tackle this problem a gel can be applied between the skin and the probe. The gel will make sure there is no air between the probe and the skin. For this application, a lossless gel with a relative permittivity approaching infinity would be ideal. This gel then has an impedance approaching 0 and effectively only the voltage drop caused by the skin impedance is measured.

2.4.1. Choice of gel

Unfortunately, no gels with permittivities approaching infinity could be found. There are however gel like substances called phantoms [13] that imitate the skin permittivity to some degree. These phantom are man-made chemical substances with specific recipes that can be tuned to achieve a given frequency response. As with any chemical substance the properties of the phantom heavily rely upon the reproducibility and stability of the production process. One of the phantoms that was given to our team, was not stable and varied heavily upon the location the probe was placed at the gel surface.

Since it is desirable to know the exact permittivity of gel, in order to be able to compensate for the effect of the interfacing gel, the phantom was not deemed to be a suitable. This compensation process is,

however, beyond the scope of this project, due to time constraints. No data on electrical properties of the gels used for ultrasonic imaging could be found as well.

The conductive gels used for making electrocardiograms and defribillation are not suitable. These gels short the inner and outer conductors of the probe and thus making measuring the skin impedance impossible.

Therefore it was decided that Vaseline should be used as interfacing gel. Vaseline is not dangerous to human skin and has a known relative permittivity of 2.16 [14], with a negligible imaginary part (and therefore is lossless) and does not vary with frequency.

2.4.2. Setting up the simulation

To determine the effect of the gel, three simulations were set up. The first simulation was the ideal case where the probe touches the skin without any air in between. This simulation is the same as displayed in fig. 2.2. The second simulation was with 1 mm Vaseline gel in between the probe and the skin and the third with 1 mm of air in between the probe and the air.

A picture of the gel simulation is displayed in fig. 2.14. In the air simulation, the gel layer was set to the permittivity of air to simulate the air gap.

2.4.3. Results

In figures 2.12 and 2.13, the effect of the gel is plotted for different skin permittivities.

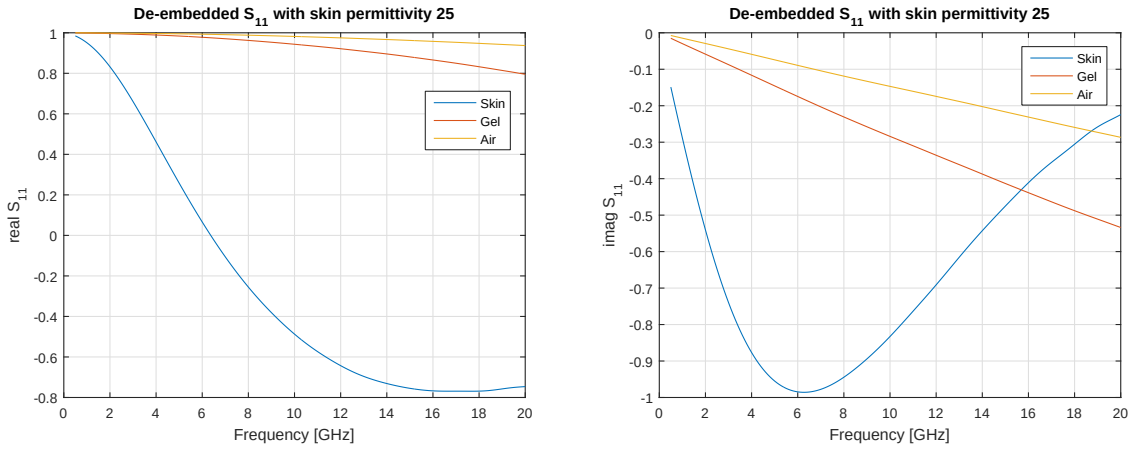

Figure 2.12: Plots of the real part of the S-parameters for skin with gel, skin with air gap and only skin, with a skin permittivity of 25

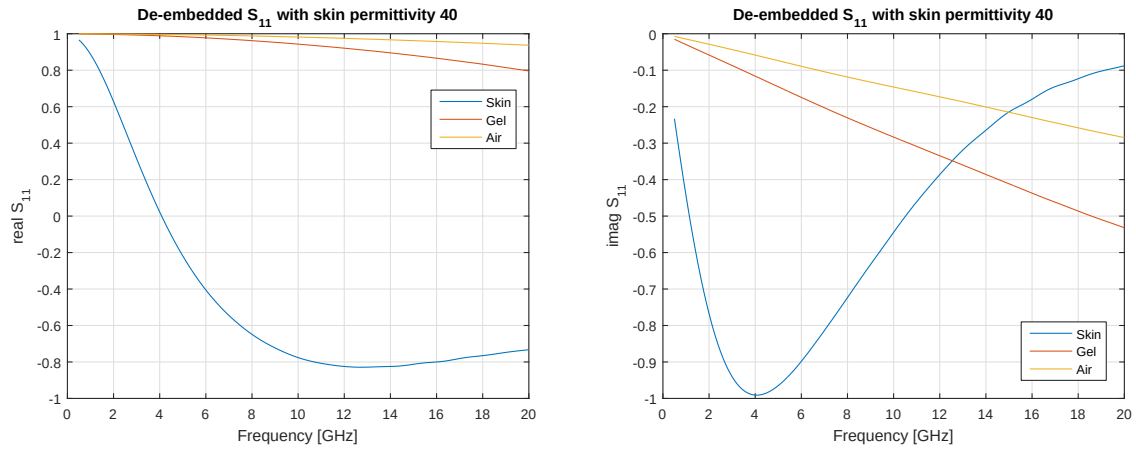

Figure 2.13: Plots of the real part of the S-parameters for skin with gel, skin with air gap and only skin, with a skin permittivity of 40

It can be seen that the skin permittivity almost does not affect the measured S-parameters. It can also be seen that the gel, because of its low relative permittivity distorts the measurements almost as much as air.

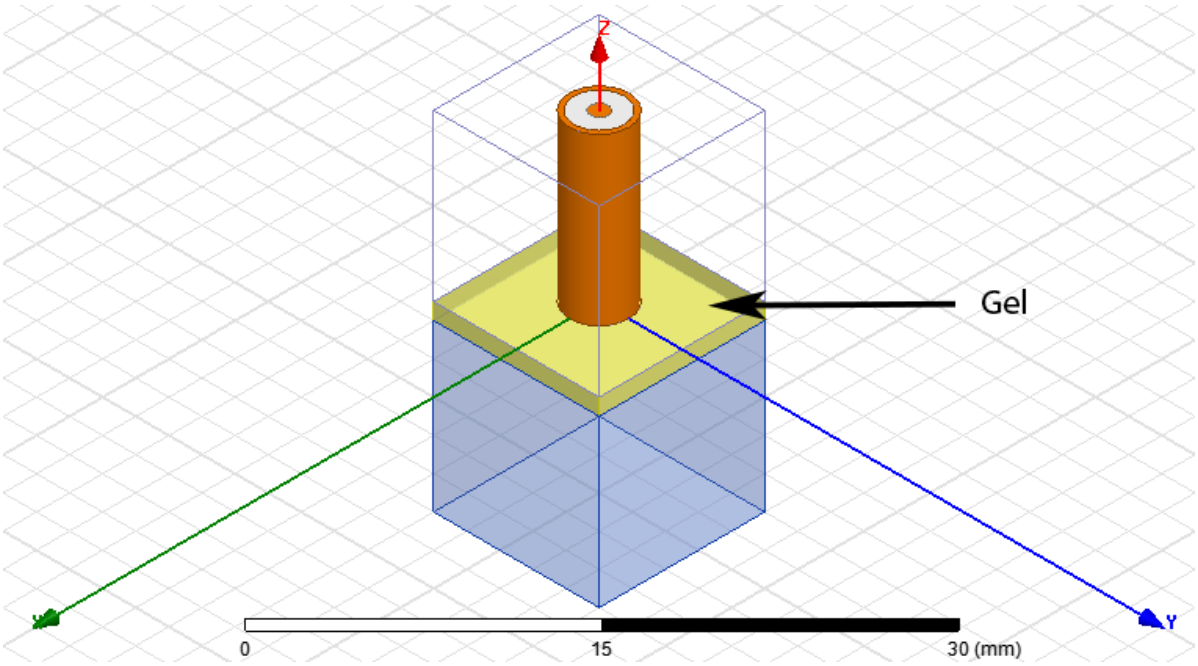

Figure 2.14: The simulation setup to determine the effect of the gel

2.5. Effect of interface cap

To keep the probe clean and sterile, there was looked into the possibility of using a protective cap that can be put on the probe. The cap can then be replaced by another one when doing measurements on another patient. In this way the probe does not directly touch the skin and thereby prevents the transfer of infections from patient to patient.

2.5.1. Choice of the cap material

The ideal cap material would be, just like the gel, a material with a relative permittivity that approaches infinity. But again, just like the gel, there were no materials found with this property. Therefore the choice was made to choose a material with known permittivity, so that if needed, the measurement results could be compensated for the effect of the cap.

A suitable material that was found, was Teflon. Teflon has a well known relative permittivity, just like Vaseline. The relative permittivity of Teflon does not vary with frequency and the dielectric loss tangent is negligible. The real part of the relative permittivity of Teflon is 2.1.

An advantage of Teflon is that its permittivity is almost equal to that of Vaseline. This ensures that almost no reflections will occur between the cap and the gel. This should make compensating for the effect of the cap in combination with the gel easier. As mentioned before in section 2.4.1, this compensation process is beyond the scope of this thesis.

Teflon is also available in many forms. There are Teflon variants that are hard, but also variants that are more flexible that for example can be used to produce tubing. This flexible Teflon would be a great material for a probe cap, since a very tight fitting cap could be made. This cap can be made slightly smaller than the probe, and stretch when the cap is put on the probe. In this way air will be pushed out so that no air will remain between the probe and the cap.

2.5.2. Setting up the simulation

To draw the cap, a cylinder was drawn around the cap. The bottom thickness of the cap was set at 1 mm. This bottom thickness was chosen to represent the worst case scenario, since it should be easily possible to manufacture Teflon caps with bottom thicknesses thinner than 1 mm.

A picture of the simulation setup can be seen in fig. 2.17.

2.5.3. Results

In figures 2.15 and 2.16, the effect of the cap is plotted.

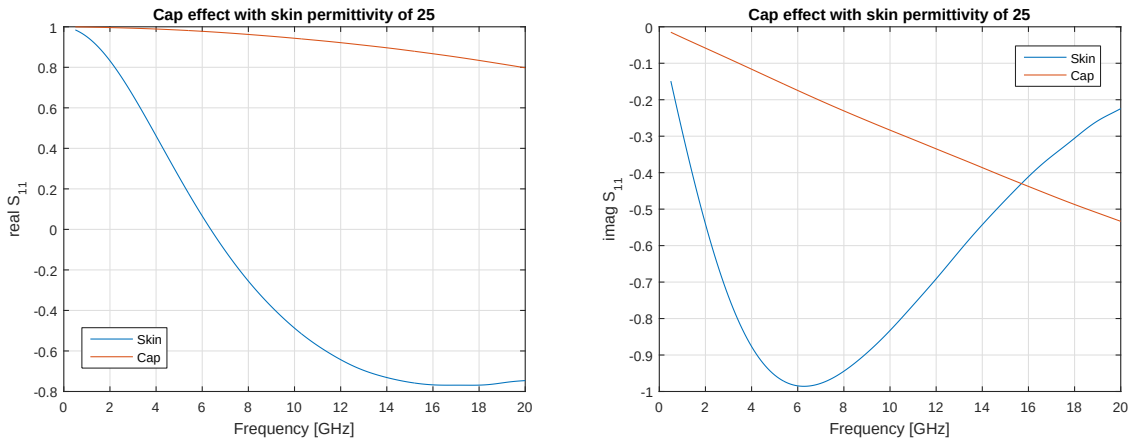

Figure 2.15: Plots of the real part of the S-parameters for the skin measured with cap in between the probe and the skin and skin measured directly. The skin permittivity in this simulation was 25

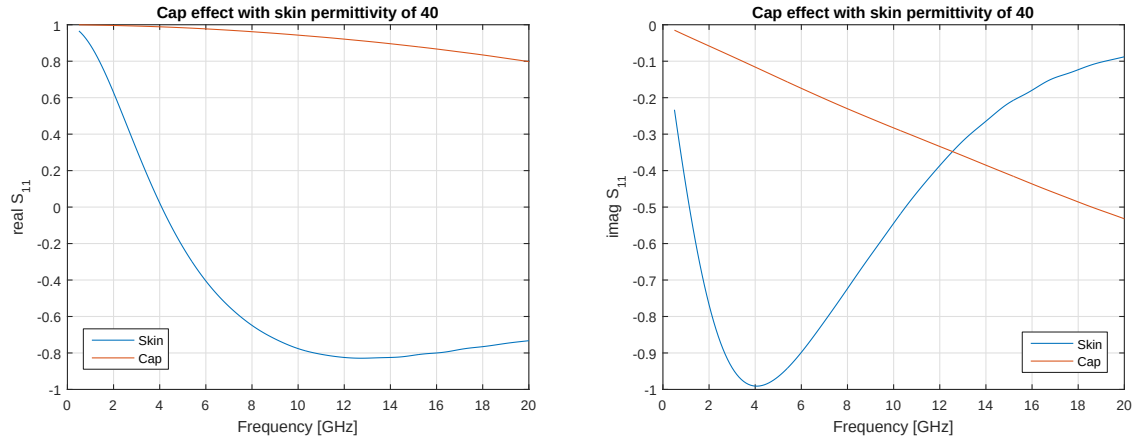

Figure 2.16: Plots of the real part of the S-parameters for the skin measured with cap in between the probe and the skin and skin measured directly. The skin permittivity in this simulation was 40

It can be seen that the cap distorts the measurements significantly. Also note that the effect of the cap is almost the same as that of the gel.

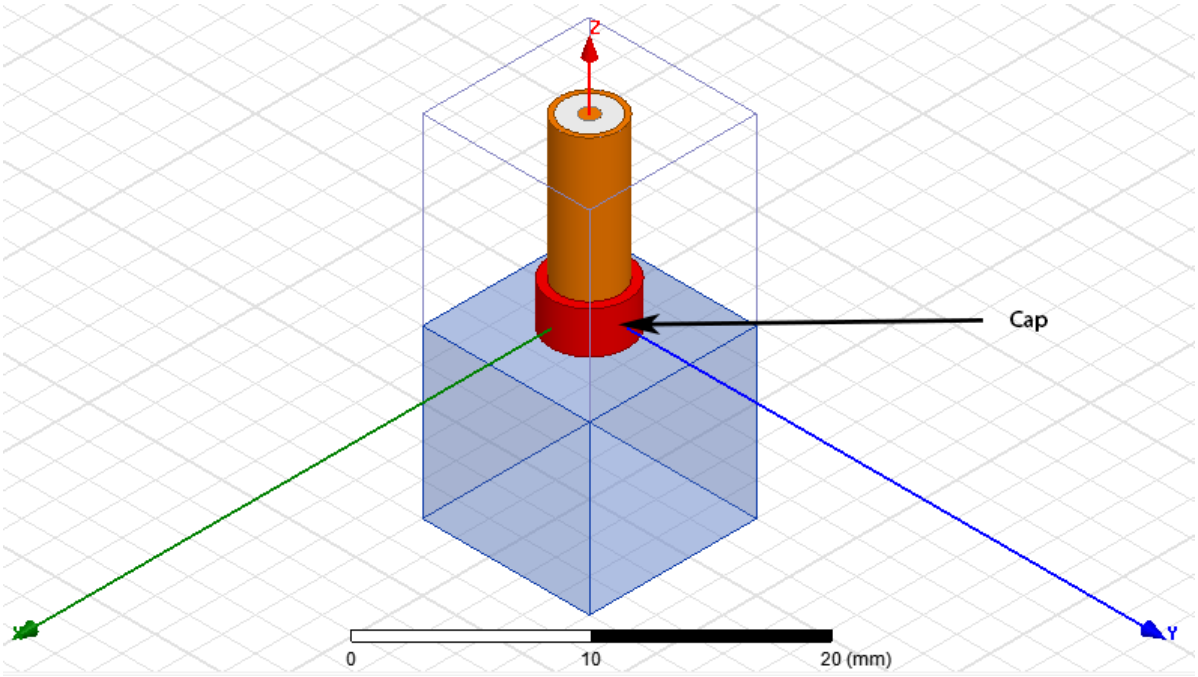

Figure 2.17: The HFSS setup for the cap simulation

3

User interface

3.1. Structure

3.1.1. Model-View-Controller

A graphical user interface (GUI) is needed to show the measured permittivity values. The GUI is designed through the Model-View-Controller (MVC) design pattern. The Model, View and Controller are the three important elements on which the software architecture design pattern is based [15], [16]. This design patterns separates the interface from the underlying logic and data. This makes it possible to show different interfaces for the same data, such as an overview and a detailed view, see fig. 3.1a.

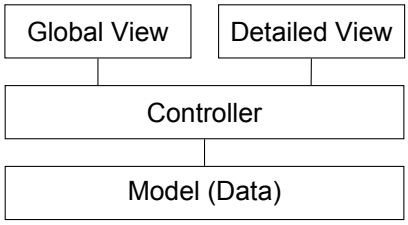

(a) The MVC pattern allows multiple views of the same data with one Controller

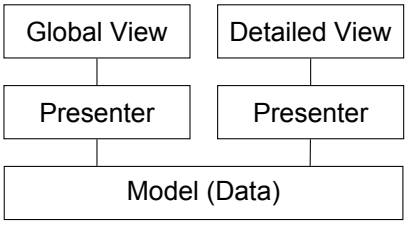

(b) The MVP pattern allows multiple views of the same data with multiple Presenters

The GUI should be easily maintainable and extendible. The modular way of MVC is a perfect fit for these requirements. New data can be added to the Model, new GUI elements or even a new interface to a View and new functionality to the Controller. The Model-View-Presenter pattern was also considered. This pattern is somewhat similar to MVC, but has a separate Presenter for each View instead of one Controller for all Views (see fig. 3.1b) and routes all the data through the Presenters. This was not chosen because a direct link between the Model and the View was desired, so no large amounts of data have to go trough the Controller. One Controller which contains all the logic was also a better fit for this GUI than separate Presenters, because there is functionality which is used by both Views.

The functionality of each of the elements of the MVC pattern is as follows:

The Model contains the data. It has no knowledge of either the Controller or the View. It has methods to set parameters and get the data from it, which can be called from the Controller, but the Model itself does not know that the Controller exists. The Model just contains the data and makes it available.

The View is the user interface and is the only part of the application the user sees. A View gets data directly from the Model. It sends user input through to the Controller and contains almost no logic.

The Controller contains all the logic and controls the Model and the View. It reacts on user input, and updates the Model and View accordingly. The Controller is the only class that has full knowledge

about all the other components. The Controller starts the Views and tells the Model and Views when to update.

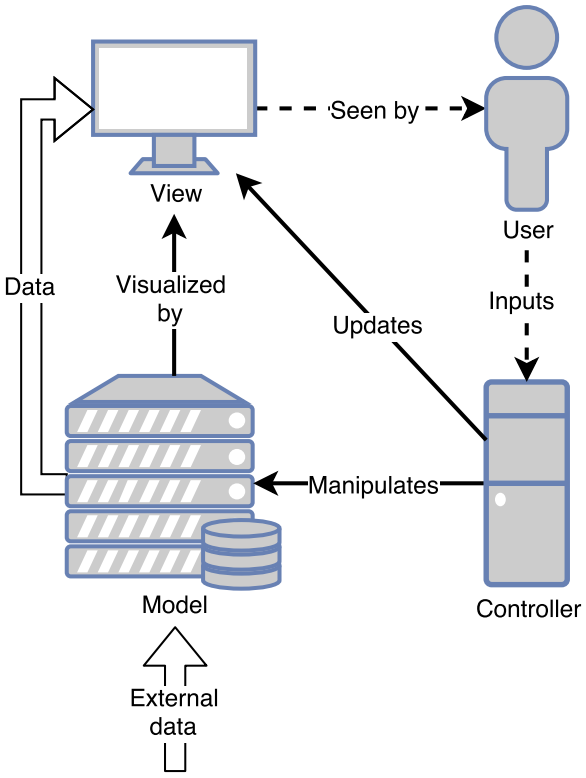

Figure 3.2: Model-View-Controller flow. The thick arrows show the data path, the dashed arrows the user interaction and the solid arrow internal interaction.

This interaction between the Controller, Model, View and the user is shown in fig. 3.2.

3.1.2. Classes

All code of the GUI is Object Oriented, with the exception of the external helper functions and libraries `setifexist`, `select3d` and `export_fig`. The four classes are shown in fig. 3.1a and explained below.

`Model`

The `Model` class stores the data in three attributes: `coor`, `e_real` and `e_imag`.

`coor` Contains the coordinates and normals of the measured points. This is a $6 \times n$ matrix, in which each row contains x, y, z, n_x, n_y and n_z.

`e_real` Contains the real parts of the measured relative permittivity values. This is an $m \times n$ matrix. Each row has the permittivity data over the frequency range. m is thus dependant on the frequency range and the step size at which the measurements are done.

`e_imag` Contains the imaginary parts of the measured relative permittivity values and is otherwise the same as `e_real`.

`Model` not only stores the data, but also has functions to work with the data:

`calculateGridData` `Model` contains the interpolation code, which can be called from the Controller.

`addData` Data can easily be added to the model through this function. This function takes a coordinate, normal and permittivity values as its parameters. The inputs can also be arrays and matrices which contain multiple measurement points.

`resetData` The data can be reset through this function.

`GlobalView`

The `GlobalView` class is the main window of the GUI. These are the most important functions in this class:

`initGUI` This function initializes the GUI elements when created and sets the callback functions of the GUI elements to the right functions in the Controller, so that when a button is clicked, the right action occurs.

`layoutUI` The GUI is resizeable. When the GUI is resized by the user, this function is called, which calculates the correct new dimensions for all UI elements. This function also decides whether to show or hide certain elements based on the user's choice.

`plotData` The data is plotted in this function. No calculations on the data are done, these are in the `Model` class. This function can be called from the Controller to refresh the data display.

`DetailView`

The `DetailView` class shows a secondary windows which contains a plot of the permittivity as a function of the frequency. The main functions of this class are similar to those of the `GlobalView` class, but smaller and less complicated since there are less GUI elements.

`Controller`

The `Controller` class manages when the other classes do something. It creates the other classes, calls their functions when needed and contains the callback function of the UI elements. These are the most important functions of this class

3.1.3. Extending the GUI

The GUI has to interact with the measuring and positioning systems. To facilitate this, easy accessible functions have been made available. The Controller contains a function to refresh the data views. The Model data can be added from external sources, and can also be reset from other classes.

There are two approaches to integrate the GUI with the measurement systems. The first approach is to control the measuring from the current Controller. An advantage of this approach is that it is easier to access functions and integrate the flow when it is within the same class. A disadvantage, however, is that this approach can lead to a very convoluted large class.

The second approach is to use a supervisor class, which manages the GUI, the positioning system and the measuring system as three large top level blocks, as shown in fig. 3.3. Each block can then be seen as a black box with a few external accessible functions, and the supervisor does not care what happens inside the box. A disadvantage of this approach is that a supervisor class and a top level GUI class are needed, which introduces two new levels through which a command has to go before it is actually executed. The major advantage, however, is that this approach is very easily manageable and extendible. It is relatively easy to add another top level block and the top level does not have to be changed when a new function is added on a lower level, since the supervisor does not see this function, only the black box.

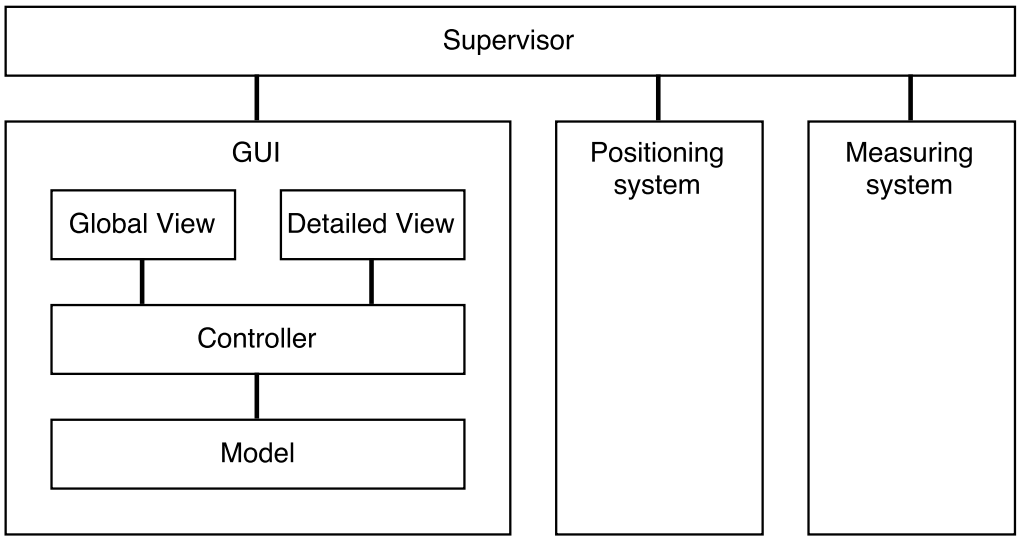

Figure 3.3: Using a Supervisor class to control the GUI, positioning and measuring systems

3.2. Implementation

3.2.1. Visual design

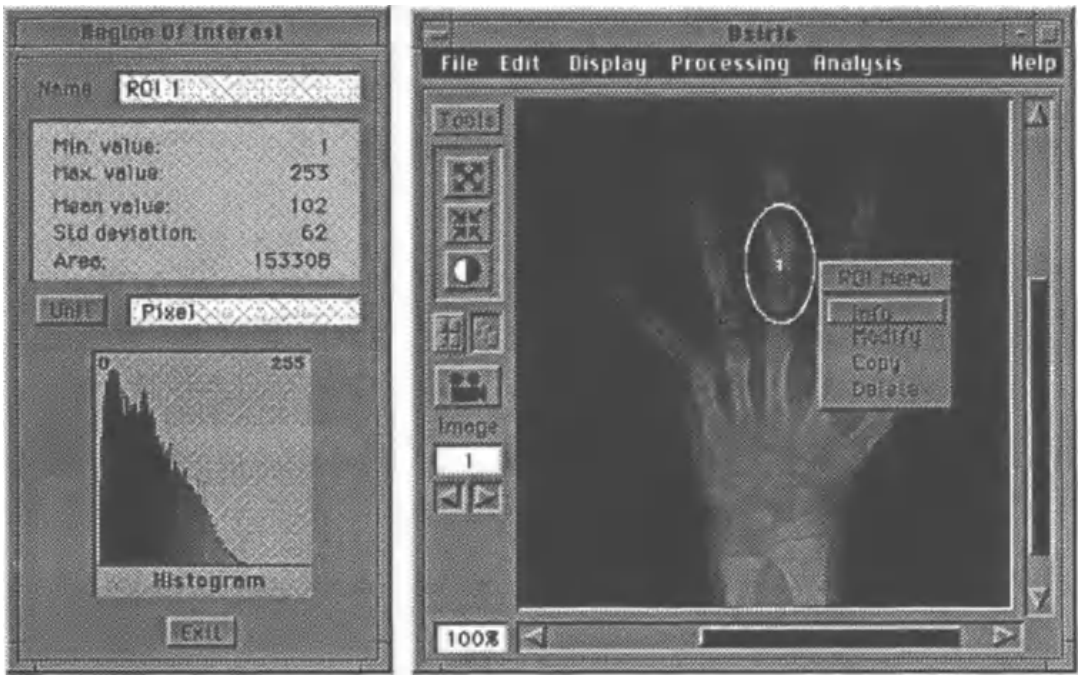

Figure 3.4: The OSIRIS User Interface

We have looked at other GUIs that display in vivo measurement data, such as MRUI [17] and OSIRIS [18]. The OSIRIS interface shows a good method of displaying detailed information next to a global visual overview, which has partially been incorporated into the TIPS GUI. This interface is shown in fig. 3.4. Smith and Mosier have written guidelines for designing user interface software. This GUI particularly uses the guidelines on graphics [19], since displaying graphical data is the main task of the software. A clear reference for the data is shown in a colourbar, the data can be zoomed and standard pictorial symbols are used, to name a few of the conventions that have been followed.

3.2.2. Functionality

The GUI of TIPS is written in MATLAB to enable easy integration with the rest of the system. The GUI (see fig. 3.6) consists of a window with a large plotting area, various push-buttons, navigation buttons, a slider, two popup menus and a text area. An optional second window contains another large plotting area (see fig. 3.7). The plot in the first window can be divided into four subplots, as is shown in fig. 3.6. Each subplot can be shown as a single large plot. This can be chosen in the popup menu in the upper right corner, which is shown in its expanded state in fig. 3.5a.

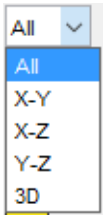

(a) Close-up of the expanded popup menu to choose a plot

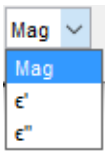

(b) Close-up of the expanded popup menu to choose which value to show

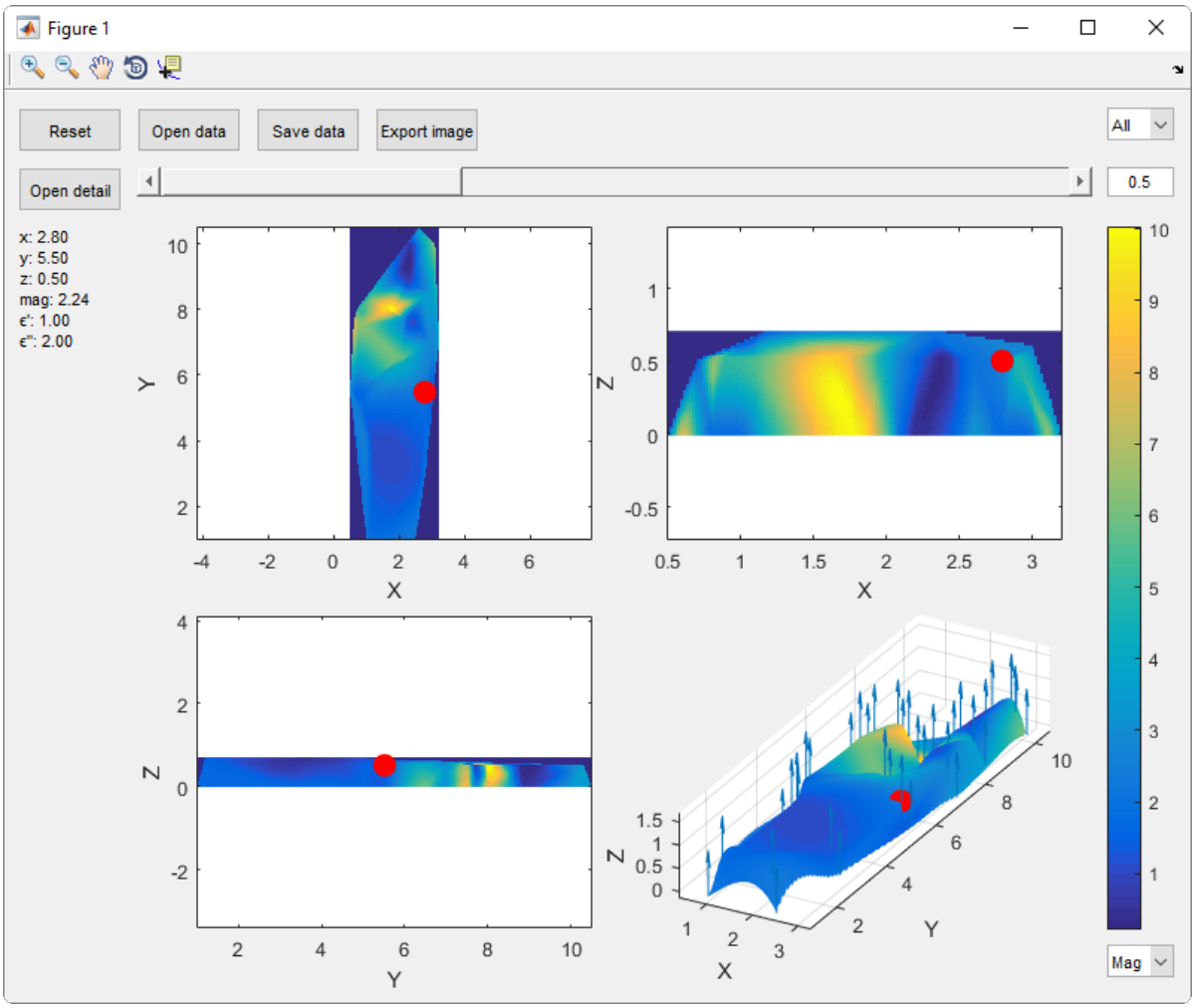

Figure 3.6: Graphical User Interface

The plots show the relative permittivity at a location, indicated by a colour, which corresponds to the colour-bar on the right. A choice can be made to show either the magnitude, the real part (ε') or the imaginary part (ε'') of the permittivity. The popup menu to make this choice is shown in fig. 3.5b.

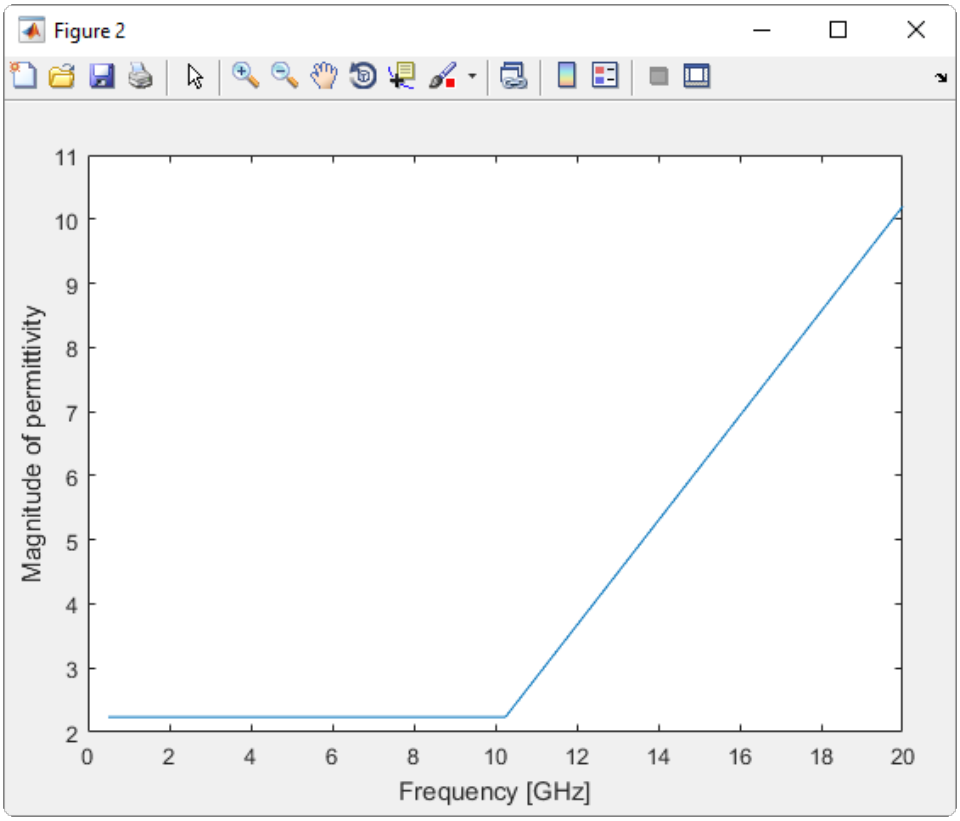

Figure 3.7: Detail view of one measurement point. This example point shows values at three frequencies (0,5 GHz, 10,25 GHz and 20 GHz).

The permittivity data over the entire frequency range is saved in the program. The frequency the user wants to view can be selected with the slider above the plot, or can be typed into the text field right to the slider. If a user inputs a frequency for which no data is available, the nearest available frequency is selected and updated in the slider and text field.

The user can select a single measurement point to see details at that position. When a user clicks in one of the plots, the nearest measured point is selected. The index of this point is found by calculating the distance from the selected coordinate to each point in an array, finding the index of the minimal distance in the array and selecting the point using this index. The distance is calculated by using the Pythagorean theorem on the difference between the clicked point and the measurement point. In MATLAB code: `[~,index] = min((p(1)-coor(:,1)).^2 + (p(2)-coor(:,2)).^2 + (p(3)-coor(:,3)).^2)`

The position of each measurement point is shown by an arrow. The orientation of the arrow matches the orientation at which the probe was held at that point.

By clicking the ‘Open detail’ button, the user can open a secondary window (fig. 3.7). This window shows a plot of the relative permittivity as a function of the frequency. Depending on the choice the user has selected in the main window, either the magnitude, the real part or the imaginary part of the permittivity is shown.

3.3. 3D plot

3.3.1. Interpolation

The application can show a 3D plot of the permittivity. However, the data only consists of points, while it is desirable to show a continuous surface. To do this, the data is interpolated in between the points. First, a grid is constructed. This is done in MATLAB with `[xq,yq] = meshgrid(xr,yr);`, where

`xr` and `yr` are $1 \times m$ and $1 \times n$ vectors with the x and y ranges of the grid. `xq` and `yq` are $n \times m$ matrices.

The data is then interpolated on this grid with the help of the MATLAB function `griddata`: `zq = griddata(x,y,z,xq,yq,'cubic')`. `x`, `y` and `z` are the original coordinates of the measured points. To calculate the interpolated permittivity values `cq = griddata(x,y,c,xq,yq,'cubic')` is used, where `c` are the original measured permittivity values. Both linear and cubic interpolation have been tried. Cubic interpolation gives a smooth surface as opposed to the ragged result of linear interpolation and was thus chosen. The difference is shown in fig. 3.8.

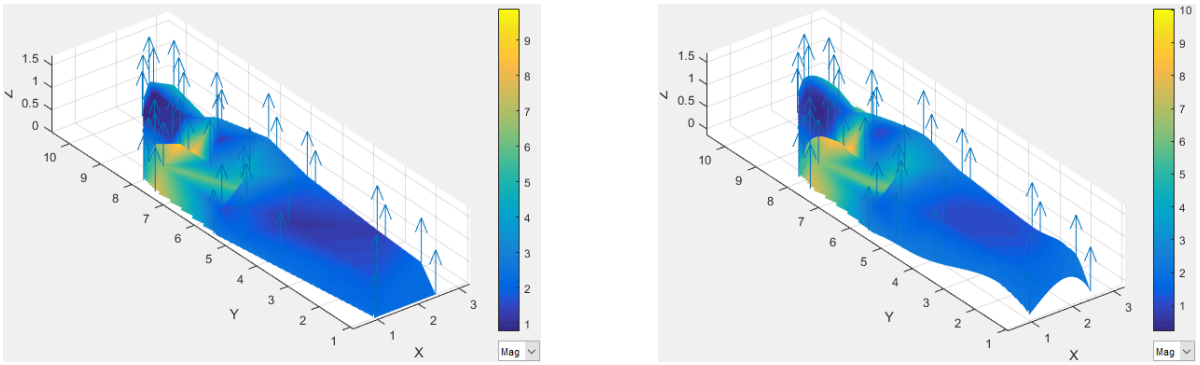

(a) Linear

(b) Cubic

Figure 3.8: Difference between interpolation techniques

The resolution of the resulting picture is dependant on the size of the grid range vectors. Higher m and n, while maintaining the limits of the grid, result in a finer grid. To determine the step size, the maximum of the distances between the maximal and minimal x, y and z coordinates is taken, and divided by the desired amount of steps: `d = max([max(x)-min()x),max(y)-min(y),max(z)-min(z)])/steps`. This ensures that the pixel size is the same in every dimension.

3.3.2. Normals and surfaces

Not only the coordinates of the measurement points are saved, but also the orientation of the probe at those points. This can help to construct a surface. The assumption can be made that the probe is held, or close to, perpendicular to the skin. This means that the orientation of the probe is the normal of the skin surface as well.

One method is to draw small squares that are perpendicular to the orientation of the probe, and use these as 3D 'pixels' to draw the surface. This is shown in fig. 3.9 The orientation is taken as the normal $\mathbf{n}$. First the cross product of the normal and a random unit vector $\hat{\mathbf{u}}$, for example [1, 0, 0], is taken, to get a vector which is perpendicular to the normal and that axis ($\mathbf{v}$). Then the cross product of that vector and the normal is taken, to get another vector which is perpendicular to the normal ($\mathbf{w}$). These two vectors, $\mathbf{v}$ and $\mathbf{w}$, span the surface. A square can then be plot around the point obtaining the vertices by subtracting or adding $\mathbf{v}$ and $\mathbf{w}$ to and from each other.

Another method to construct a surface from normals is described by Basri, Jacobs and Kemelmacher [20, sec. 4]. The normal of a surface is the unit vector consisting of the scaled partial derivatives of the surface at that point:

$$(n_x, n_y, n_z) = \frac{1}{\sqrt{z_x^2 + z_y^2 + 1}}(z_x, z_y, 1) \qquad (z_z = 1) \tag{3.1}$$

The following expressions for z_x and z_y can be obtained from this:

$$z_x = \frac{n_x}{n_z} \tag{3.2a}$$

$$z_y = \frac{n_y}{n_z} \tag{3.2b}$$

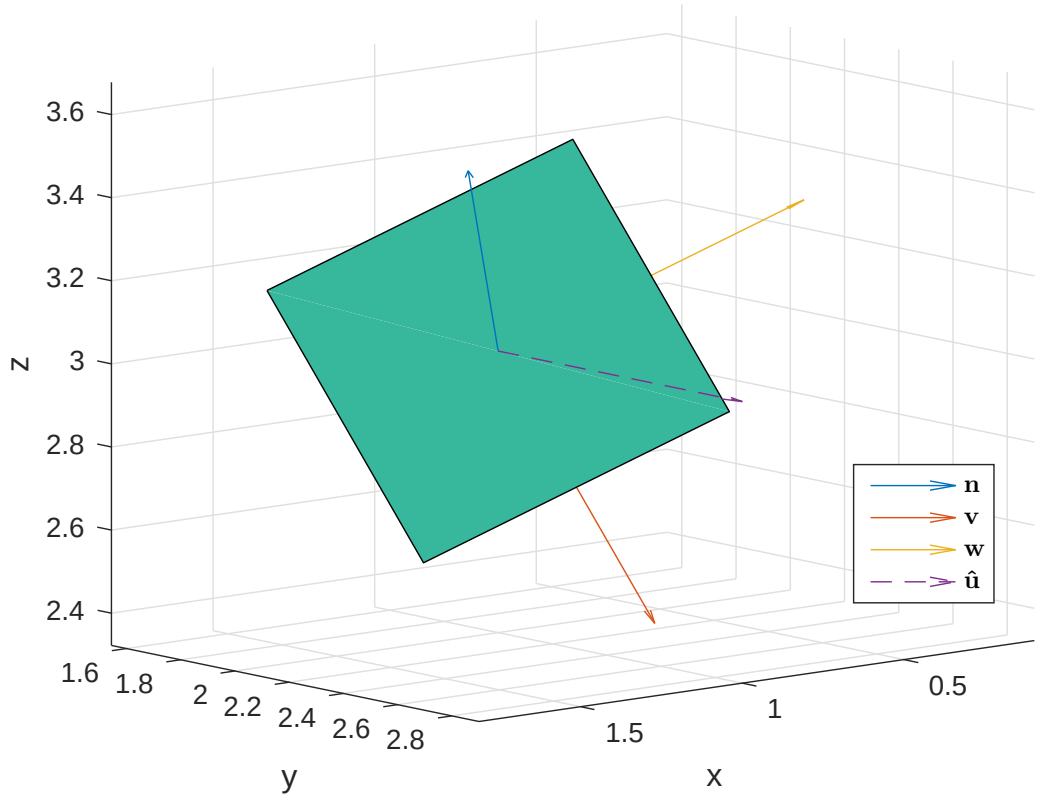

Figure 3.9: Surface perpendicular to normal

On a grid, z_x and z_y can be written as

$$z_x \approx z(x+1,y) - z(x,y) \tag{3.3a}$$
$$z_y \approx z(x,y+1) - z(x,y) \tag{3.3b}$$

Combining eq. (3.1) and eq. (3.3) gives the system of equations for z:

$$n_z z(x+1,y) - n_z z(x,y) = n_x \tag{3.4a}$$
$$n_z z(x,y+1) - n_z z(x,y) = n_y \tag{3.4b}$$

This system can be solved if one $z(x_0, y_0)$ is known, or a linear least square approximation can be used if the system is overdetermined, which is the case if multiple $z(x,y)$ values are known. This method requires the normals at all points on the grid te be known. These normals can be calculated using the same interpolation method as described above.

We have tried to apply this method based on one known $z(x,y)$, $z(1,1)$ was taken as 0 as reference. The results were not good, however. There were a lot of a large spikes, especially around the edges, since n_z is small there. These spikes can be seen in fig. 3.10. Basri, Jacobs and Kemelmacher suggest a method to solve these problems around the edges. From eq. (3.2) is comes that $\frac{z_x}{z_y} = \frac{n_x}{n_y}$. An additional constraint around the edges can follow from this:

$$n_y(z(x,y) - z(x+1,y)) = n_x(z(x,y) - z(x,y+1)) \tag{3.5}$$

This constraint was not successfully implemented due to time constraints.

A least squares approximation of the surface can be made by taking the known $z(x,y)$ values and applying the normals as constraints to the fit. Since the components of the normal are equal to the

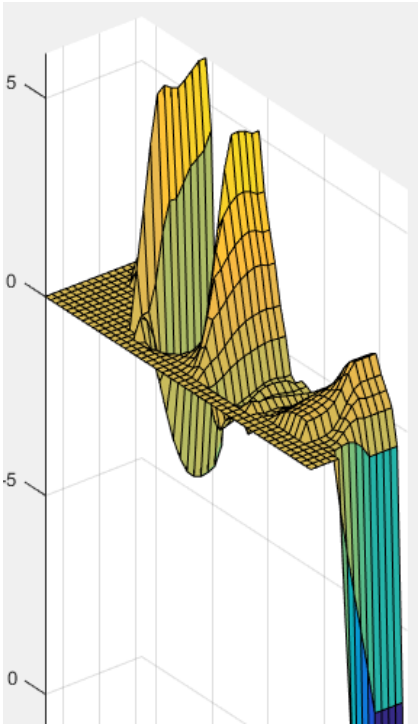

Figure 3.10: 3D surface with spikes

partial derivative of the surface, the constraint $\frac{\partial z(x,y)}{\partial x} = n_x(x,y)$ and $\frac{\partial z(x,y)}{\partial y} = n_y(x,y)$, where n_x and n_y are properly scaled, can be applied for every known normal to refine the surface fit. We were not able to implement this in the interpolation within the available time for this project.

The two methods to construct a 3D surface using not only the coordinates of the measured points, but also the orientation of the probe at that point, both were not successful. Therefore it was chosen to use only the interpolation technique described in section 3.3.1 in this project. The 3D surface was thus successfully constructed from the measured points, but could be improved in the future by using one of the above mentioned methods.

4

Conclusion

4.1. Skin interface

The data generated by the simulations for the lookup table and determination of standard coefficients seem to have worked well. Truong and Kremers [4] were able to accurately derive the permittivity of an unknown substance (propanol) by using the data generated by the simulations.

Due to the optimization step, it was possible to successfully run simulations without exceeding memory limitations and simulation time smaller than 2 hours per design variation and still acquire accurate results.

Unfortunately, the results of the Vaseline gel were disappointing. It can be seen in figs. 2.12 and 2.13 that the gel distorts the measurements significantly, and does not improve the measurements that much in comparison to the air gap scenario. The same goes for the cap, the Teflon cap distorts the measurements as well for the same reason the gel does, namely the low permittivity.

Although optimization process sped the simulation times up, due to time constraints it was not possible to look into the gel and the cap more. Given more time, there could be looked into the actual impact of a gel with a very high permittivity on the measurements using HFSS. This should greatly increase the capacitance of the gel and therefore reduce the effect on the measurements.

If possible, it would have been interesting to some buy tubes of ultrasound imaging gels produced in different batches of the same manufacturer and measure its electrical properties. This way the consistency of these gels can be checked and because they often have high water content, they might be a good choice for a interfacing gel.

It would be also nice to see what the effect of reducing the cap thickness would be. By decreasing the thickness, the capacitance increases and the impedance thus decreases. Therefore the effect of the cap should be also less and a reasonable thickness that does not distort the measurements significantly could be determined.

Another interesting matter that could have been looked into with more time is generating a dataset with more data points for the lookup table in order to obtain even more accurate derivation of permittivities.

A suggestion for improvement of the spatial resolution of the skin permittivity measurement system is that there could be looked into the possibility of using multiple measurements from different locations (since location data is already available) in a later stadium of the research. For this, there may be looked at astronomy since techniques for combining images are widely used in that field already.

4.2. User interface

The user interface has been successfully implemented. The MVC design pattern has been applied and results in a clear divided program code. The code is easily extendible due to the modular approach and

the clear helper functions within the classes. The GUI is able to plot all measured data in a consistent manner, while not overwhelming the user, through the use of some user selectable options.

Part of the GUI is a 3D plot of the measured data. It was desirable to construct this 3D surface in such a way that not only the positions of the measured points, but also the orientation of the probe at these points would be taken into account. Two methods were identified to accomplish this. The first constructed a 3D surface out of discreet squares positioned in 3D space, which act as 3D pixels. However, no suitable method was found to make a closed surface and to detect where these square planes intersect, when extended. The second method expresses the height of a 3D surface as a function of the components of the normal of the surface. The normal at each point can be calculated by interpolating the known normals at the measured points. This method constructs a system of equations which can solved when the proper boundary conditions are applied or to which a surface can be fitted with a least squares fit. Solving the system directly gave spikes in the surface at places where the z-component of the normal was small. An attempt to fit the surface to the system with additional constraints applied was unsuccessful because, due to limited time, a correct fitting system could not be constructed.

Future work can explore and refine this method. It can be researched how to apply constraints to the partial derivatives of a surface. Once a system describing these constraints has been constructed, a least squares fit can be applied to the system to fit an optimal 3D surface through the measured points instead of the current interpolation.

Further work can also implement the extension of the classes to include a structure with a supervising class, which also encompasses the measuring and position tracking systems.

A

Code

A.1. Matlab code

A.1.1. Complex permittivity to dielectric loss tangent conversion

```
%% Permittivity real and imaginary part to dielectric loss tangent
   conversion
%
%   This script calculates the dielectric loss tangent using the complex
%   and real parts of the permittivity so this data can be used by HFSS.
%   The data is automatically written to .tab files so the datasets can be
%   easily loaded into HFSS.
%
% Written by Wietse Bouwmeester at 22-5-2016

clear all;
load all_permittivities.mat;

butanol_loss = fopen('[FILENAME]', 'w');
butanol_permittivity = fopen('[FILENAME]', 'w');

methanol_loss = fopen('[FILENAME]', 'w');
methanol_permittivity = fopen('[FILENAME]', 'w');

water_loss = fopen('[FILENAME]', 'w');
water_permittivity = fopen('[FILENAME]', 'w');

propanol_loss = fopen('[FILENAME]', 'w');
propanol_permittivity = fopen('[FILENAME]', 'w');

ethanol_loss = fopen('[FILENAME]', 'w');
ethanol_permittivity = fopen('[FILENAME]', 'w');

for i = 1:size(butanol,1)
   fprintf(butanol_permittivity, '%i\t%i\n', butanol(i,1), butanol(i,2));
   fprintf(butanol_loss, '%i\t%i\n', butanol(i,1), (butanol(i,3) ./
      butanol(i,2)));
end

for i = 1:size(methanol,1)
```

```
    fprintf(methanol_permittivity, '%i\t%i\n', methanol(i,1), methanol(i,2)
        );
    fprintf(methanol_loss, '%i\t%i\n', methanol(i,1), (methanol(i,3) ./
        methanol(i,2)));
end

for i = 1:size(water,1)
    fprintf(water_permittivity, '%i\t%i\n', water(i,1), water(i,2));
    fprintf(water_loss, '%i\t%i\n', water(i,1), (water(i,3) ./ water(i,2)))
        ;
end

for i = 1:size(ethanol,1)
    fprintf(ethanol_permittivity, '%i\t%i\n', ethanol(i,1), ethanol(i,2));
    fprintf(ethanol_loss, '%i\t%i\n', ethanol(i,1), (ethanol(i,3) ./
        ethanol(i,2)));
end

for i = 1:size(propanol,1)
    fprintf(propanol_permittivity, '%i\t%i\n', propanol(i,1), propanol(i,2)
        );
    fprintf(propanol_loss, '%i\t%i\n', propanol(i,1), (propanol(i,3) ./
        propanol(i,2)));
end

fclose('all');
```

A.1.2. File generation for HFSS parametric sweep

```
%% Parametric sweep generator for HFSS
%
%   This script generates a file that contains all desired variations of
%   dielectric loss tangent and the real part of the relative permittivity
%   for generating reference data.
%
% Written by Wietse Bouwmeester at 3-6-2016

clear;

%Open file to write to
loss_tangent = fopen('[FILENAME]', 'w');
fprintf(loss_tangent, '%s\t%s\n', '$epsilon', '$loss');

for e_prime = 1:2:41;

    %Generate requested parameters
    epsilon = [ e_prime.*ones(1,21) ; 0:15/20:15];

    for i = 1:size(epsilon,2)
        fprintf(loss_tangent, '%i\t%i\n', e_prime, (epsilon(2,i)./epsilon
            (1,i)));
    end

end
fclose('all');
```

B

Simulation

B.1. Simulation setup

B.1.1. General Setup instructions

First the model needs to be created. The first part of the model that will be drawn is the coaxial probe.

In order to draw the outer conductor, first a cylinder with its origin at the coordinates (0,0,0) is added to the design. The radius of this cylinder is chosen to be 1,7907 mm, equal to the radius of the coaxial probe that is used for measuring the permittivity of the skin material. The height of this cylinder is set to 10 mm. Next, the dielectric is created by drawing a cylinder with again (0,0,0) as point of origin and with a height matching that of the outer conductor. The radius is chosen to be 1,5 mm. A copy of the dielectric is subtracted from the cylinder that represents the outer conductor.

A similar process needs to be repeated in order to draw the inner conductor. The inner conductor has a radius of 0,254 mm and subsequently a copy of this inner conductor is subtracted from the dielectric. Lastly, the materials of the drawn objects need to be designated. The inner and outer conductors are assigned the HFSS standard material copper and the dielectric is assigned the standard Teflon material.

Next up, the air box is drawn. To do this, a box of 10 mm by 10 mm by 10 mm is drawn with its point of origin at (−5 mm,−5 mm,0). The box extends 10 mm in the $+z$-direction. To make sure the coaxial probe and the air box do not overlap, a copy of the coaxial probe needs to be subtracted from the air box. Lastly, the material of this air box is set to vacuum.

The last object to be drawn is the skin material. This is done by drawing a box of 10 mm by 10 mm by 10 mm. This cube has again (−5 mm,−5 mm,0) as point of origin but extends 10 mm in the -z direction. HFSS does not contain a pre-installed material that resembles skin, so this material needs to be added manually. This option can be found in the materials window. The relative permittivity of this skin material is set to 22. This is about the lower boundary of the relative permittivity of dry skin according to Andreuccetti, Fossi and Petrucci [11].

Now the model is finished, excitations and boundary conditions need to be assigned. The face of the dielectric on the top side of the coaxial probe is assigned a wave port excitation. This is in order to properly excite the coaxial cable with TEM mode propagation as would be the case in reality. HFSS will calculate the S-parameters as seen from this port.

Next, the faces of the air box and the skin material on the outside of the model are assigned the radiation boundary condition. This conditions emulates infinite space around the design and thus ensuring no reflections from the outer faces of the model occur.

If this boundary conditions is not assigned, HFSS will assume the perfect E boundary condition. This condition can be imagined as a shell of a perfect conducting material covering the outside faces of

the design. This is in this case not desired since it does not reflect the real situation, contrary to the radiation boundary condition which does this much better.

Finally, the variables of the parameters need to be set. First, the solution type of HFSS is set to modal solution. Secondly the analysis setup was added. The highest frequency that measurement equipment will measure is 20 GHz, so this will be also the highest frequency HFSS needs to calculate S-parameters at. According to the HFSS user guide [21] the solution frequency should be set to the upper frequency in the sweep, because the mesh size will be the smallest for this frequency and therefore it should work with lower frequencies as well.

The convergence settings were set to a maximum delta S of 0.02 and the target was set to three converged passes. Also the sweep setup needs to be added to the analysis setup. The sweep parameters are set so that a range of 0,5 GHz to 20 GHz in steps of 100 MHz will be executed. The sweep type is set to discrete to enable simulation of frequency dependant materials, that will be used in simulations for among others calculations of error terms.

Now HFSS is ready to calculate the S-parameters at the top of the probe. However, the desired S-parameters are the ones measured at the skin/bottom of the probe instead of on the top of the probe. The effect on the S-parameters of the coaxial probe thus needs to be compensated for. This process is called de-embedding. To do de-embedding, the S-matrices of the coaxial probe need to be obtained. This is done by copying the HFSS-design and deleting the air box and the skin material so only the coaxial probe is left. Next, to obtain the S-matrix, a wave port needs to be added to the bottom side of the probe. Running the simulation will now give the S-matrix rather than just the reflection coefficient.

B.1.2. Calibration setup

First the general model described in section 2.1.1 was adapted. The probe was extended 5 mm below the box that previously represented the skin, and now represents the liquid. Also, a copy of the probe was subtracted from the material that represents the liquid so that there would be no overlap between the probe and the liquid. A picture of the design is shown in fig. 2.5.

The de-embedding model was adjusted as well. Because the coaxial probe got 5 mm longer, this also needed to be done in the calibration simulation setup.

Thereafter, the measured permittivity needed to be assigned to the liquid. The measured data that was delivered was a file that contained the real part of the relative permittivity (ε') and the imaginary part of the relative permittivity (ε''). ε'' needs to be converted to the dielectric loss tangent using the script in appendix A.1.1. The output data can than be imported as dataset into HFSS and assigned to the liquid as material parameter.

B.1.3. Lookup table setup

Again the general setup was modified. In this simulation, only the relative permittivity of the skin had to vary. Instead of setting the relative permittivity of the skin material to a number, it was set to a variable. Thereafter, a parametric sweep was added to the design. In the parametric setup a sweep of the above set variable was configured. This sweep ranges from 1 to 40 in steps of 1. The simulation was now ready to be executed and would execute a frequency sweep in steps of 0,1 GHz between 0,5 GHz and 20 GHz (196 points) for each of the 40 different relative permittivities.

B.1.4. Gel setup

To determine the effect of the gel, multiple simulations were set up. The first simulation is equal to the general case described in appendix B.1.1. This simulation was used as the reference, since this one represents the ideal case with no air between the probe and the skin.

The second simulation that was made, was the case with air between the probe and the skin. This was done by moving the skin material the air gap length down, and expanding the air box so that touched the skin again.

The last simulation is the simulation with the Vaseline gel. The skin material was moved down just like the second simulation set up, but instead of expanding the air box the gel material was added. This was done by drawing a box between the air box and the skin material filling up the left over space, see fig. 2.14. To represent the worst case scenario for the gel, the thickness of gel was chosen at 1 mm.

The gel permittivity was set to 2.16, and the dielectric loss tangent was set to 0. A parametric sweep was added to check the effect of gel in combination with varying skin permittivity as well. The parametric sweep was set up to sweep over the real part of the relative permittivity of the skin from 25 to 40 in steps of 5.

B.1.5. Cap setup

In order to determine the effect of the cap on the measurements, a new HFSS setup was made. Just as in section 2.4.2 the skin material was moved 1 mm down.

After that, a cylinder was drawn with its origin at (0, 0, −1 mm). The radius of this cylinder was chosen to be 2,3 mm, so that the walls of the cap would be 0,5 mm thick. The cap height was set at 2,5 mm.

Thereafter, the air box was expanded down so it touched the skin material. To remove overlap of the cap with the probe and the air box, a copy of the cap was subtracted from the air box and a copy of the probe was subtracted from the cap.

Now a cap of with a bottom thickness 1 mm was finished. This bottom thickness was chosen to represent the worst case scenario, since it should be possible to manufacture Teflon caps with bottom thicknesses thinner than 1 mm.

Lastly, a parametric sweep was set up for the skin permittivity. Two permittivity values were chosen, namely 25 and 40, since these are about respectively the lowest and highest values the skin permittivity can be. A picture of the simulation setup can be seen in fig. 2.17.

Bibliography

[1] Integraal Kankercentrum Nederland. (Feb. 2016). Cijfers over kanker, Incidentie huid, [Online]. Available: http://www.cijfersoverkanker.nl/selecties/Incidentie_huid/img575ddb9ad788e (visited on 12/06/2016).

[2] C. M. Balch, S.-J. Soong, J. E. Gershenwald, J. F. Thompson, D. S. Reintgen, N. Cascinelli, M. Urist, K. M. McMasters, M. I. Ross, J. M. Kirkwood, M. B. Atkins, J. A. Thompson, D. G. Coit, D. Byrd, R. Desmond, Y. Zhang, P.-Y. Liu, G. H. Lyman and A. Morabito, 'Prognostic factors analysis of 17,600 melanoma patients: Validation of the american joint committee on cancer melanoma staging system', *Journal of Clinical Oncology*, vol. 19, no. 16, pp. 3622–3634, 15th Aug. 2001. PMID: 11504744.

[3] A. Breslow, 'Thickness, cross-sectional areas and depth of invasion in the prognosis of cutaneous melanoma', *Annals of Surgery*, vol. 172, no. 5, pp. 902–908, Nov. 1970, ISSN: 0003-4932. DOI: 10.1097/00000658-197011000-00017. PMID: 5477666.

[4] M. H. Truong and A. W. Kremers, 'Calibration procedure for complex permittivity extraction using open-ended coaxial probe', Bachelor Thesis, TU Delft, Jun. 2016.

[5] C. Treffers and L. van Wietmarschen, 'Position and orientation determination of a probe with use of the IMU MPU9250 and a ATmega328 microcontroller', Bachelor Thesis, TU Delft, Jun. 2016.

[6] *IEEE standard definitions of terms for radio wave propagation*, IEEE Std. 211-1997, IEEE, 1998. DOI: 10.1109/IEEESTD.1998.87897.

[7] S. J. Orfanidis, 'Electromagnetic waves and antennas', in. ECE Department Rutgers University 94 Brett Road Piscataway, NJ 08854-8058: Rutgers University, 2008, ch. 14, pp. 664–708. [Online]. Available: http://www.ece.rutgers.edu/~orfanidi/ewa/ch14.pdf.

[8] H. Mitchell, T. Hamilton, F. Steggerda and H. Bean, 'The chemical composition of the adult human body and its bearing on the biochemistry of growth', *The Journal of Biological Chemistry*, vol. 158, pp. 625–637, 1st May 1945.

[9] J. L. Schepps and K. R. Foster, 'The uhf and microwave dielectric properties of normal and tumour tissues: Variation in dielectric properties with tissue water content', *Phys. Med. Biol.*, vol. 25, no. 6, pp. 1149–1159, 17th Mar. 1980.

[10] D. Popovic, L. McCartney, C. Beasley, M. Lazebnik, M. Okoniewski, S. C. Hagness and J. H. Booske, 'Precision open-ended coaxial probes for in vivo and ex vivo dielectric spectroscopy of biological tissues at microwave frequencies', *IEEE Transactions on Microwave Theory and Techniques*, vol. 53, no. 5, pp. 1713–1722, May 2005, ISSN: 0018-9480. DOI: 10.1109/TMTT.2005.847111.

[11] D. Andreuccetti, R. Fossi and C. Petrucci. (1997). An internet resource for the calculation of the dielectric properties of body tissues in the frequency range 10 Hz – 100 GHz. Based on data published by C.Gabriel et al. in 1996, IFAC-CNR, [Online]. Available: http://niremf.ifac.cnr.it/tissprop/.

[12] A. P. Gregory and R. N. Clarke, 'Tables of the complex permittivity of dielectric reference liquids at frequencies up to 5 GHz', National Physical Laboratory, Tech. Rep., Jan. 2012. [Online]. Available: http://www.npl.co.uk/content/conpublication/4295 (visited on 08/06/2016).

[13] M. Lazbnik, E. L. Madsen, G. R. Frank and S. C. Hagness, 'Tissue-mimicking phantom materials for narrowband and ultrawideband microwave applications', *PHYSICS IN MEDICINE AND BIOLOGY*, no. 50, Aug. 2005. [Online]. Available: http://uwcem.ece.wisc.edu/pdf/lazebnik_pmb05.pdf (visited on 10/06/2016).

[14] S. A. Alshehri, S. Khatun, A. B. Jantan, R. R. Abdullah, R. Mahmood and Z. Awang, 'Experimental study of breast cancer detection using UWB imaging', *International Journal on Advanced Science, Engineering and Information Technology*, vol. 1, no. 1, pp. 83–87, 2011, ISSN: 2088-5334. DOI: 10.18517/ijaseit.1.1.20.

[15] G. E. Krasner and S. T. Pope, 'A description of the Model-View-Controller user interface paradigm in the Smalltalk-80 system', *Journal of Object-Oriented Programming*, vol. 1, pp. 26–49, 3 1988, ISSN: 0896-8438.

[16] F. Buschmann, R. Meunier, H. Rohnert, P. Sommerlad and M. Stal, *Pattern-Oriented Software Architecture, A System of Patterns*. 1996, pp. 123–143, ISBN: 0471958897.

[17] A. Naressi, C. Couturier, R. d. B. I. Castang and D. Graveron-Demilly, 'Java-based graphical user interface for MRUI, a software package for quantitation of in vivo/medical magnetic resonance spectroscopy signals', *Computers in Biology and Medicine*, vol. 31, no. 4, pp. 269–286, Jul. 2001. DOI: 10.1016/s0010-4825(01)00006-3.

[18] Y. Ligier, M. Funk, O. Ratib, R. Perrier and C. Girard, 'The OSIRIS user interface for manipulating medical images', in *Picture Archiving and Communication Systems (PACS) in Medicine*, Springer Science + Business Media, 1990, pp. 395–398. DOI: 10.1007/978-3-642-76566-7_60.

[19] S. L. Smith and J. N. Mosier, *Guidelines For Designing User Interface Software*. Massachusetts, USA: The MITRE Corporation Bedford, 1986, pp. 141–174, ISBN: 1-800-295-6354.

[20] R. Basri, D. Jacobs and I. Kemelmacher, 'Photometric stereo with general, unknown lighting', *Internation Journal of Computer Vision*, vol. 72, no. 3, pp. 239–257, May 2007. DOI: 10.1007/s11263-006-8815-7.

[21] Ansoft Corporation, *Ansoft high frequency structure simulator v10 user's guide*, version 1.0, 225 West Station Square Drive, Suite 200, Pittsburgh PA 15219, USA, 21st Jun. 2005. [Online]. Available: http://anlage.umd.edu/HFSSv10UserGuide.pdf.